Article

SOURCE DATA | TRANSPARENT PROCESS

THE EMBO JOURNAL

Msp1/ATAD1 maintains mitochondrial function by facilitating the degradation of mislocalized tail-anchored proteins

Yu-Chan Chen[1], George K E Umanah[2,3], Noah Dephoure[4], Shaida A Andrabi[2,3], Steven P Gygi[4], Ted M Dawson[2,3,5,6], Valina L Dawson[2,3,5,7] & Jared Rutter[1,*]

Abstract

The majority of ER-targeted tail-anchored (TA) proteins are inserted into membranes by the Guided Entry of Tail-anchored protein (GET) system. Disruption of this system causes a subset of TA proteins to mislocalize to mitochondria. We show that the AAA+ ATPase Msp1 limits the accumulation of mislocalized TA proteins on mitochondria. Deletion of *MSP1* causes the Pex15 and Gos1 TA proteins to accumulate on mitochondria when the GET system is impaired. Likely as a result of failing to extract mislocalized TA proteins, yeast with combined mutation of the *MSP1* gene and the GET system exhibit strong synergistic growth defects and severe mitochondrial damage, including loss of mitochondrial DNA and protein and aberrant mitochondrial morphology. Like yeast Msp1, human ATAD1 limits the mitochondrial mislocalization of PEX26 and GOS28, orthologs of Pex15 and Gos1, respectively. GOS28 protein level is also increased in *ATAD1*$^{-/-}$ mouse tissues. Therefore, we propose that yeast Msp1 and mammalian ATAD1 are conserved members of the mitochondrial protein quality control system that might promote the extraction and degradation of mislocalized TA proteins to maintain mitochondrial integrity.

Keywords AAA+ ATPase; Guided Entry of Tail-anchored protein; mitochondrial protein quality control; tail-anchored proteins
Subject Categories Membrane & Intracellular Transport; Metabolism
DOI 10.15252/embj.201487943 | Received 19 January 2014 | Revised 22 April 2014 | Accepted 24 April 2014 | Published online 19 May 2014
The EMBO Journal (2014) 33: 1548–1564

See also: **RS Hedge** (July 2014)

Introduction

Tail-anchored (TA) proteins are a distinct subset of membrane proteins, which are uniquely characterized by a single transmembrane domain (TMD) at the C-terminus with the majority of the protein extending into the cytoplasm. They play critical roles in a variety of cellular processes including intracellular trafficking (e.g., all SNARE proteins), protein translocation and maturation (e.g., Sec61β, Tom5, Tom6, Tom7, and Tom22), apoptosis (e.g., Bcl2 family), organelle ultrastructure (e.g., Fis1), and metabolism (e.g., CPT1, Cyb5) (Wattenberg & Lithgow, 2001; Borgese *et al*, 2003). The majority of TA proteins are targeted to two distinct membrane systems: the mitochondrial outer membrane and the ER membrane from where TA proteins can be subsequently sorted to the nuclear envelope, Golgi complex, peroxisome, vacuole/lysosome, and plasma membrane, probably by vesicle-mediated trafficking (Kutay *et al*, 1995).

The topology of TA proteins precludes them from being targeted by the canonical co-translational signal recognition particle pathway that is used by the vast majority of membrane proteins (Kutay *et al*, 1995; Steel *et al*, 2002; Yabal *et al*, 2003; Brambillasca *et al*, 2005). Instead, a post-translational targeting system, GET (Guided Entry of Tail-anchored proteins), or TRC (TMD Recognition Complex) in *Saccharomyces cerevisiae* (yeast) or mammals, respectively, chaperones newly synthesized TA proteins and mediates their insertion into the ER membrane (Stefanovic & Hegde, 2007; Schuldiner *et al*, 2008; Hegde & Keenan, 2011; Denic, 2012). The mechanism whereby TA proteins are targeted and inserted into mitochondria has not yet been determined. In yeast, the GET system starts with capture of the nascent TA protein by the pre-targeting subcomplex composed of Get4, Get5, and Sgt2 (Jonikas *et al*, 2009; Wang *et al*, 2010). Via interaction with Get4, Get3 binds the cargo protein complex and binds the TA protein by directly associating with the TMD (Chartron *et al*, 2010; Wang *et al*, 2010). Through docking of

1 Department of Biochemistry, University of Utah School of Medicine, Salt Lake City, UT, USA
2 Neuroregeneration and Stem Cell Programs, Institute for Cell Engineering, Johns Hopkins University School of Medicine, Baltimore, MD, USA
3 Department of Neurology, Johns Hopkins University School of Medicine, Baltimore, MD, USA
4 Department of Cell Biology, Harvard Medical School, Boston, MA, USA
5 Solomon H. Snyder Department of Neuroscience, Johns Hopkins University School of Medicine, Baltimore, MD, USA
6 Departments of Pharmacology and Molecular Sciences, Johns Hopkins University School of Medicine, Baltimore, MD, USA
7 Department of Physiology, Johns Hopkins University School of Medicine, Baltimore, MD, USA
*Corresponding author. Tel: +1 801 581 3340; Fax: +1 801 581 7959; E-mail: rutter@biochem.utah.edu

Get3 onto the ER membrane receptor, a Get1/Get2 heterodimer, the TA protein is then released and properly inserted (Schuldiner *et al*, 2008; Wang *et al*, 2010; Mariappan *et al*, 2011). However, the fidelity of protein targeting is not perfect, and when it is impaired by mutation (e.g., of the GET system), TA proteins mislocalize to the cytosol or mitochondria (e.g., peroxisomal Pex15 and ER Ubc6) (Schuldiner *et al*, 2008; Jonikas *et al*, 2009). To this end, a protein quality control system has evolved to clear TA protein aggregates from the cytosol (Hessa *et al*, 2011). We hypothesized that a parallel system evolved to clear TA proteins that have mislocalized to the mitochondria and constituted a threat to mitochondrial function.

The mitochondrion is a complex organelle that performs functions that are fundamental to many aspects of cell biology. Therefore, failure or dysregulation of this organelle is associated with many forms of human disease. This includes cancer (Kroemer & Pouyssegur, 2008), diabetes (Patti & Corvera, 2010), neurodegenerative disease (Lessing & Bonini, 2009), and others (Lopez-Armada *et al*, 2013; Lopez-Otin *et al*, 2013). This critical importance necessitates that cells employ a multi-tiered quality control system to maintain the integrity of mitochondria (Rugarli & Langer, 2012). One line of defense consists of intra-mitochondrial proteases that enable the degradation of misfolded or damaged proteins. Among them, two AAA+ (ATPase Associated with various cellular Activities) proteases, *m*-AAA and *i*-AAA, enforce protein quality in the matrix and inter-membrane space compartments, respectively (Gerdes *et al*, 2012; Janska *et al*, 2013). They are characterized by a AAA+ domain that, in most cases, oligomerizes to form a channel to unfold protein substrates using the energy derived from ATP hydrolysis. Unfolded polypeptides are subsequently degraded by an associated proteolytic domain (Sauer & Baker, 2011). Mutations affecting these proteases cause a plethora of phenotypes in yeast, including respiratory deficiency, loss of mitochondrial DNA (mtDNA), altered mitochondrial morphology, and decreased chronological lifespan (Thorsness *et al*, 1993; Campbell *et al*, 1994; Janska *et al*, 2013). Cells employ a related quality control system on the mitochondrial outer membrane, which enables the extraction and proteasomal degradation of proteins exposed to the cytosol (Taylor & Rutter, 2011). This system appears to also utilize the AAA+ ATPase, Cdc48 in yeast or p97 in mammals, for protein extraction prior to engagement of the proteasome (Heo *et al*, 2010; Tanaka *et al*, 2010; Xu *et al*, 2011). When mitochondria depolarize, cells initiate the autophagic degradation of mitochondria or mitophagy as a second line of defense (Youle & Narendra, 2011; Ashrafi & Schwarz, 2013). In animals, neurons seem to be particularly sensitive to the presence of damaged mitochondria. An increasing number of neurodegenerative diseases, including spastic paraplegia, spinocerebellar ataxia, Parkinson's disease, Alzheimer's disease, and peripheral neuropathies, are linked with defective mitochondrial quality control systems (Rugarli & Langer, 2012).

As a result of our ongoing project to functionally annotate the mitochondrial proteome (Hao *et al*, 2009; Heo *et al*, 2010; Bricker *et al*, 2012; Chen *et al*, 2012), we here describe the previously unknown function of Ygr028 (or Msp1) in yeast and ATAD1 (also known as Thorase) in mammals, which are mitochondrial members of the AAA+ family of proteins (Zhang *et al*, 2011). Our data suggest that they are components of the mitochondrial protein quality control system and play a crucial role in degrading TA proteins that escape from the GET system to mislocalize to mitochondria. Depletion of Msp1 in yeast or ATAD1 in human cells and mice leads to ectopic accumulation of a subset of TA proteins that mislocalize to mitochondria. We also showed that Msp1 and ATAD1 physically interact with these same mislocalized TA proteins. Finally, loss of this system causes severe mitochondria damage including respiratory deficiency, loss of mitochondria, and altered mitochondrial morphology. As a result, we hypothesize that Msp1 and ATAD1 are novel mitochondrial protein quality control components that might extract and facilitate the degradation of mislocalized TA proteins from the mitochondria.

Results

Msp1 is an evolutionarily conserved mitochondrial outer membrane protein

Protein sequence alignment and domain prediction of yeast Msp1, fly CG5395, mouse ATAD1, and human ATAD1 suggested that they all contain a transmembrane domain near the N-terminus and a highly conserved AAA+ domain toward the C-terminus (Fig 1A). Because yeast Msp1 was previously annotated as a mitochondrial protein (Nakai *et al*, 1993), we first confirmed its mitochondrial localization. We generated a yeast strain co-expressing a fully functional Msp1-GFP fusion protein from the native *MSP1* promoter and mitochondrial RFP (Mito-RFP) (see Supplementary Fig S2A; the construct fully complements the growth phenotype of the *get3*Δ *msp1*Δ mutant strain, which will be discussed in the next section and Fig 2). As shown in Fig 1B, we observed a nearly complete overlap of RFP and GFP, demonstrating mitochondrial localization of Msp1-GFP. We also observed extra-mitochondrial GFP puncta (marked by arrows), however, which we showed to be peroxisomes based on co-localization with an RFP protein fused with a peroxisomal targeting sequence (SKL) (Supplementary Fig S1A).

To determine in which mitochondrial compartment Msp1 resides, we performed a biochemical fractionation experiment using a strain expressing a fully functional Msp1-His_6-HA_3 fusion protein from the native *MSP1* promoter (see Supplementary Fig S2A). Msp1 was absent from the post-mitochondria supernatant, but present in purified mitochondria. When we subjected intact, hypotonically swollen or Triton X-100 lysed mitochondria to Proteinase K digestion, Msp1 was completely degraded in all three situations, like the mitochondrial outer membrane protein Fzo1 (Fig 1C). Furthermore, similar to Om45 and Por1, both integral mitochondrial membrane proteins, neither high salt nor alkaline carbonate extracted Msp1 from mitochondria, suggesting that it is an integral mitochondrial outer membrane protein (Fig 1D).

To confirm that the mitochondrial localization of this protein family is conserved in higher eukaryotes, we established a number of human cell lines that stably express human ATAD1 (hATAD1) as a C-terminal GFP fusion. As shown in Fig 1E and Supplementary Fig S1B, the GFP signal overlapped with the mitochondrial fluorescent dye, Mitotracker Red. Consistent with yeast Msp1, we also observed that hATAD1-GFP localized to extra-mitochondrial puncta, which were verified to be peroxisomes by co-localization with a peroxisomal RFP marker (Supplementary Fig S1C). We also observed some cytoplasmic localization of ATAD1 (Supplementary Fig S1B and C). Taken together, the aforementioned data indicate

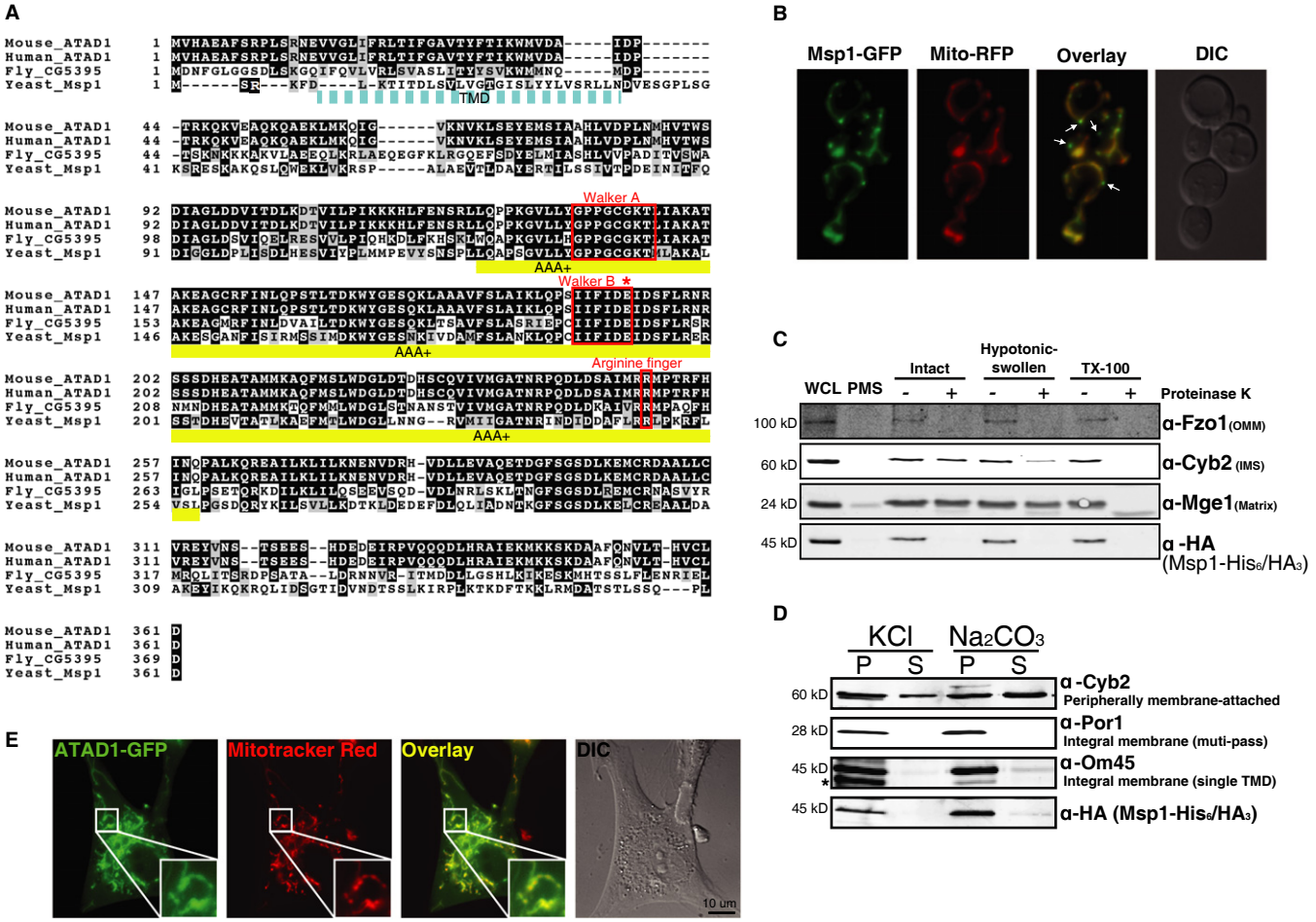

Figure 1. Msp1 is a conserved mitochondrial outer membrane protein.

A Protein sequence alignment and domain prediction of yeast, fly, mouse, and human homologs (SDSC Biology Workbench). The transmembrane domain (TMD) is marked by a dashed cyan box (dashed because the endpoints of the TMD are not clearly defined), and the AAA+ domain is marked by a yellow box. Glutamate 193 is indicated by an asterisk (*).

B Representative images of the *msp1*Δ mutant expressing Msp1-GFP and Mito-RFP. Yeast were grown to early log phase at 30°C in synthetic glucose (SD) medium and visualized by fluorescence microscopy. Peroxisomal Msp1-GFP signal is marked by arrows.

C Intact, hypotonically swollen and Triton X-100-solubilized mitochondria of the *msp1*Δ mutant expressing Msp1-His_6/HA_3 were treated with (+) or without (−) Proteinase K and analyzed by immunoblot with whole-cell lysate (WCL) and post-mitochondrial supernatant (PMS). Mge1, Cyb2, and Fzo1 are matrix, intermembrane space (IMS), and outer membrane proteins (OMM), respectively.

D Soluble (S) and pellet fraction (P) of the KCl- or Na_2CO_3-treated mitochondria purified from the strain described in (C) were analyzed by immunoblot. Cyb2 is a peripherally attached mitochondrial inner membrane protein; Por1 and Om45 are both integral outer membrane proteins. The asterisk (*) indicates a non-specific band.

E Human dermal fibroblasts (HDFs) stably expressing ATAD1-GFP were stained with Mitotracker Red and visualized by florescence microscopy.

Source data are available online for this figure.

that yeast Msp1 and human ATAD1 localize to multiple cellular compartments. Specifically, yeast Msp1 resides on the mitochondrial outer membrane, probably anchored via the N-terminal TMD, with the majority of the protein including the AAA+ domain exposed to cytosol. While Msp1 and hATAD1 might have important peroxisomal (or cytoplasmic for ATAD1) functions, this study will primarily focus on their roles in mitochondria.

The *msp1*Δ mutant exhibits synthetic growth and mitochondrial defects in combination with *GET* mutants

We generated yeast mutants lacking *MSP1*, which did not show any significant growth phenotype in regular laboratory growth conditions (Fig 2A). Two independent synthetic genetic array experiments, however, both suggested that an *msp1*Δ mutant exhibits a strong negative genetic interaction with *get2*Δ or *get3*Δ mutants (lacking critical components of the GET system), indicating that the growth of the double-mutant strain is more severely compromised than predicted from the phenotypes of the single knockouts (Costanzo *et al*, 2010; Hoppins *et al*, 2011). To verify these data, we generated *get2*Δ *msp1*Δ and *get3*Δ *msp1*Δ double-deletion strains and found that both double mutants showed more severe growth phenotypes than the single mutants when grown on glucose at 30°C, which was exacerbated at 37°C (Fig 2A, top panel). Both double mutants completely failed to grow on glycerol medium, which necessitates mitochondrial respiration for growth, whereas

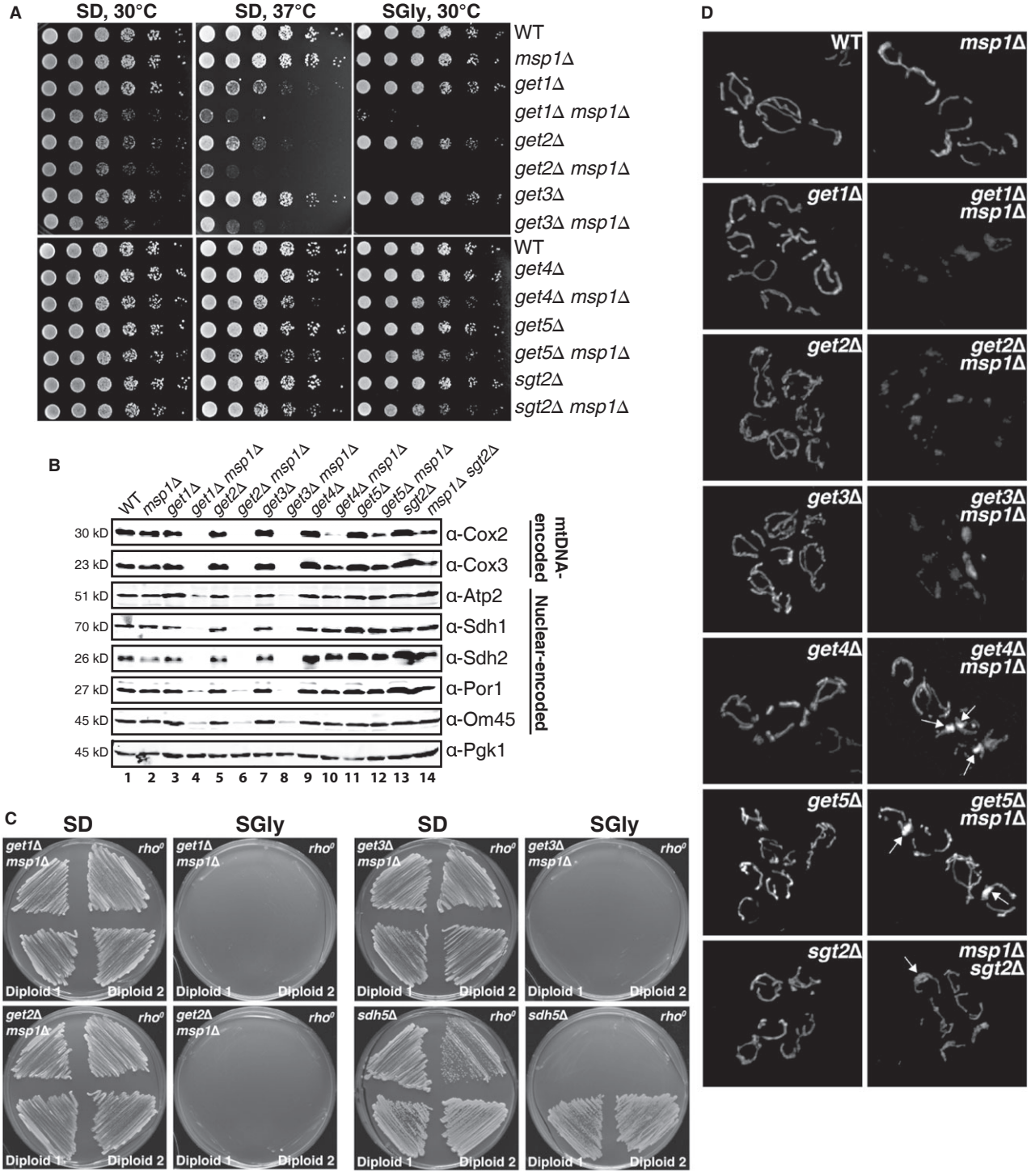

Figure 2. The *msp1Δ* mutant exhibits growth defects and severe mitochondria damage when combined with the *GET* mutants.

A Five-fold dilutions of the indicated yeast strains grown in SD medium were spotted on SD or synthetic glycerol plates (SGly) and incubated at 30 or 37°C.

B Whole-cell lysates of log-phase cultures harvested from synthetic raffinose medium were analyzed by immunoblot. Both mitochondrial and nuclear DNA-encoded mitochondrial proteins were immunoblotted. Pgk1 is a cytoplasmic control protein.

C The parental haploids and two independent diploids were streaked on SD and SGly plates and cultured at 30°C. The *sdh5Δ* strain is a control representing a respiratory deficient *rho*$^+$ strain.

D Representative images of the indicated yeast strains expressing the mito-RFP construct, grown in SD medium to log phase and visualized by fluorescence microscopy. Areas of atypical mitochondrial swelling are indicated by arrows (see also Supplementary Fig S2E). The RFP image intensity was adjusted to be similar for visualization purposes. Unadjusted images from similar exposure times are shown in Supplementary Fig S2F.

Source data are available online for this figure.

all of the single mutants exhibited wild-type growth (Fig 2A, top panel). These growth phenotypes are fully rescued by plasmid expression of the native or C-terminally tagged Msp1 protein, but not by expression of the N-terminally tagged Msp1 protein (which presumably fails to localize to mitochondria) or Msp1^{E193Q}, which is predicted to lack ATPase activity (Supplementary Fig S2A and B). In fact, expression of the Msp1^{E193Q} causes dominant-negative growth impairment when expressed in a *get3*Δ mutant (Supplementary Fig S2B). Given the functions of Get2 and Get3, it is reasonable to speculate that *MSP1* might have a similar genetic relationship with other *GET* genes including *GET1*, *GET4*, *GET5,* and *SGT2*. As expected, the synthetic growth phenotype of the *get1*Δ *msp1*Δ mutant is identical to that of the *get2*Δ *msp1*Δ and *get3*Δ *msp1*Δ double mutants (Fig 2A, top panel). The *get4*Δ *msp1*Δ, *get5*Δ *msp1*Δ, and *msp1*Δ *sgt2*Δ mutants exhibited modest synthetic growth defects, particularly on glycerol medium (Fig 2A, bottom panel). This is consistent with the published observations that Get1, Get2, and Get3 are more central players in the GET system, while Get4, Get5, and Sgt2 play a more auxiliary role (Jonikas *et al*, 2009).

The complete failure of *get1*Δ *msp1*Δ, *get2*Δ *msp1*Δ, and *get3*Δ *msp1*Δ mutants to grow on glycerol medium suggested that mitochondrial function might be impaired. To explore a potential mitochondrial phenotype further, we extracted whole-cell lysates from the wild-type (WT) and single and double mutants and immunoblotted for proteins that localize to different mitochondrial compartments (Fig 2B). We observed that the *get1*Δ *msp1*Δ, *get2*Δ *msp1*Δ, and *get3*Δ *msp1*Δ mutants were completely devoid of the mtDNA-encoded proteins, Cox2 and Cox3, and were severely depleted of all nuclear-encoded mitochondrial proteins examined, Atp2, Sdh1, Sdh2, Por1, and Om45 (Lane 4, 6, and 8). The other three double-mutant strains exhibited a partial depletion of some proteins, particularly those encoded by mtDNA (Lane 10, 12 and 14). The respiratory growth defect of the *get1*Δ *msp1*Δ, *get2*Δ *msp1*Δ, and *get3*Δ *msp1*Δ strains was also irreversible as transformation of an Msp1-expressing plasmid failed to restore the growth phenotype (Supplementary Fig S2C). We suspected that these double mutants might have lost their mitochondrial DNA and become *rho*^{0}. To directly test this, we employed a classic cross-complementation test and found that the strains lacking *MSP1* and one of the *GET* genes failed to complement the growth phenotype of a *rho*^{0} tester strain on glycerol medium (Fig 2C). These data demonstrate that the *get1*Δ *msp1*Δ, *get2*Δ *msp1*Δ, and *get3*Δ *msp1*Δ strains lack functional mtDNA. While mtDNA depletion could explain the loss of mtDNA-encoded proteins, it causes a much less severe depletion of nuclear-encoded mitochondrial proteins (Supplementary Fig S2D).

Finally, we directly visualized mitochondria by expressing Mito-RFP in the WT and single- and double-mutant strains (Fig 2D). In addition to the expected observation that the mitochondrial RFP signal in the *get1*Δ *msp1*Δ, *get2*Δ *msp1*Δ, and *get3*Δ *msp1*Δ strains was much weaker than WT or the single mutants (Supplementary Fig S2F), we also found that they exhibited severely altered mitochondrial morphology. Again, the severity of the morphological changes cannot be explained by the lack of mtDNA, which has only modest effects on mitochondrial morphology (Supplementary Fig S2E). The *get4*Δ *msp1*Δ, *get5*Δ *msp1*Δ, and *msp1*Δ *sgt2*Δ strains did not have overt morphological changes, but did have some areas of apparent atypical mitochondrial swelling (marked by arrows, Fig 2D and Supplementary Fig S2G). In summary, we have found that the combined impairment of Msp1 and the GET system causes severe mitochondrial damage, including depletion of resident proteins, loss of the mitochondrial genome, and aberrant morphology.

Depletion of mammalian *ATAD1* causes mitochondrial damage

Because a large fraction of human ATAD1 localizes to mitochondria, we wanted to assess whether this mitochondrial function is also conserved in higher eukaryotes. We tested whether depletion of ATAD1 compromises mitochondrial function. First, we performed immunoblots on lysates from brain, which was previously shown to highly express *ATAD1*, of the WT and *ATAD1*$^{-/-}$ mice (Fig 3A and B) (Zhang *et al*, 2011). We observed a significant decrease of many mitochondrial proteins in the *ATAD1*$^{-/-}$ brain of both female and male mice. The diminished mitochondrial content is further supported by the decreased basal and mitochondrial respiratory capacity of the mouse embryonic fibroblasts (MEFs) lacking *ATAD1* (Fig 3C). Second, we also directly visualized mitochondrial morphology of *ATAD1*$^{-/-}$ MEFs. While WT MEFs exhibit tubular mitochondria, we observed that the mitochondria of *ATAD1*$^{-/-}$ MEFs were severely fragmented (Fig 3D). The same mitochondrial fragmentation was observed in *ATAD1* knockdown HeLa cells (Supplementary Fig S3). Therefore, we conclude that mammalian ATAD1, similar to yeast Msp1, plays an important role in mitochondrial function.

As a complementary test of the conservation of the mitochondrial function of the Msp1 protein family, we expressed human *ATAD1* and *Drosophila melanogaster CG5395* under control of the yeast *ADH1* promoter and found that they either partially or fully rescued the growth phenotype of the *get3*Δ *msp1*Δ mutant, respectively (Fig 3E). The glycerol growth defect was also particularly suppressed, suggesting that the mitochondrial role of this protein family spans across the eukaryotic kingdom.

Msp1/hATAD1 is required to minimize the level of the TA protein Pex15/PEX26 mislocalized to mitochondria

Potential mechanisms that might underlie the severe mitochondrial defects caused by combined loss of Msp1 and the GET system were not clear. One potential connection, however, was the previous observation that disruption of the GET system causes some TA proteins to aggregate in the cytoplasm and others to mislocalize to mitochondria (Schuldiner *et al*, 2008; Jonikas *et al*, 2009). Perhaps, loss of Msp1 causes mitochondria to be particularly sensitive to the damaging effects of TA protein mislocalization to mitochondria found upon impairment of the GET system. Considering that Msp1 is part of the AAA+ protein family that, in most cases, extracts, disassembles, or unfolds protein substrates, we hypothesized that Msp1 might extract TA proteins that mislocalize to mitochondria upon loss of the GET system. We tested this hypothesis for Pex15, a peroxisomal TA protein that mislocalizes to mitochondria upon disruption of the GET system (Schuldiner *et al*, 2008; Jonikas *et al*, 2009). Surprisingly, *msp1*Δ single mutants displayed significant mitochondrial localization of a GFP-Pex15 fusion, nearly identical to previous observations with the *get3*Δ single mutant (Fig 4A) (Schuldiner *et al*, 2008; Jonikas *et al*, 2009). Much of the Pex15

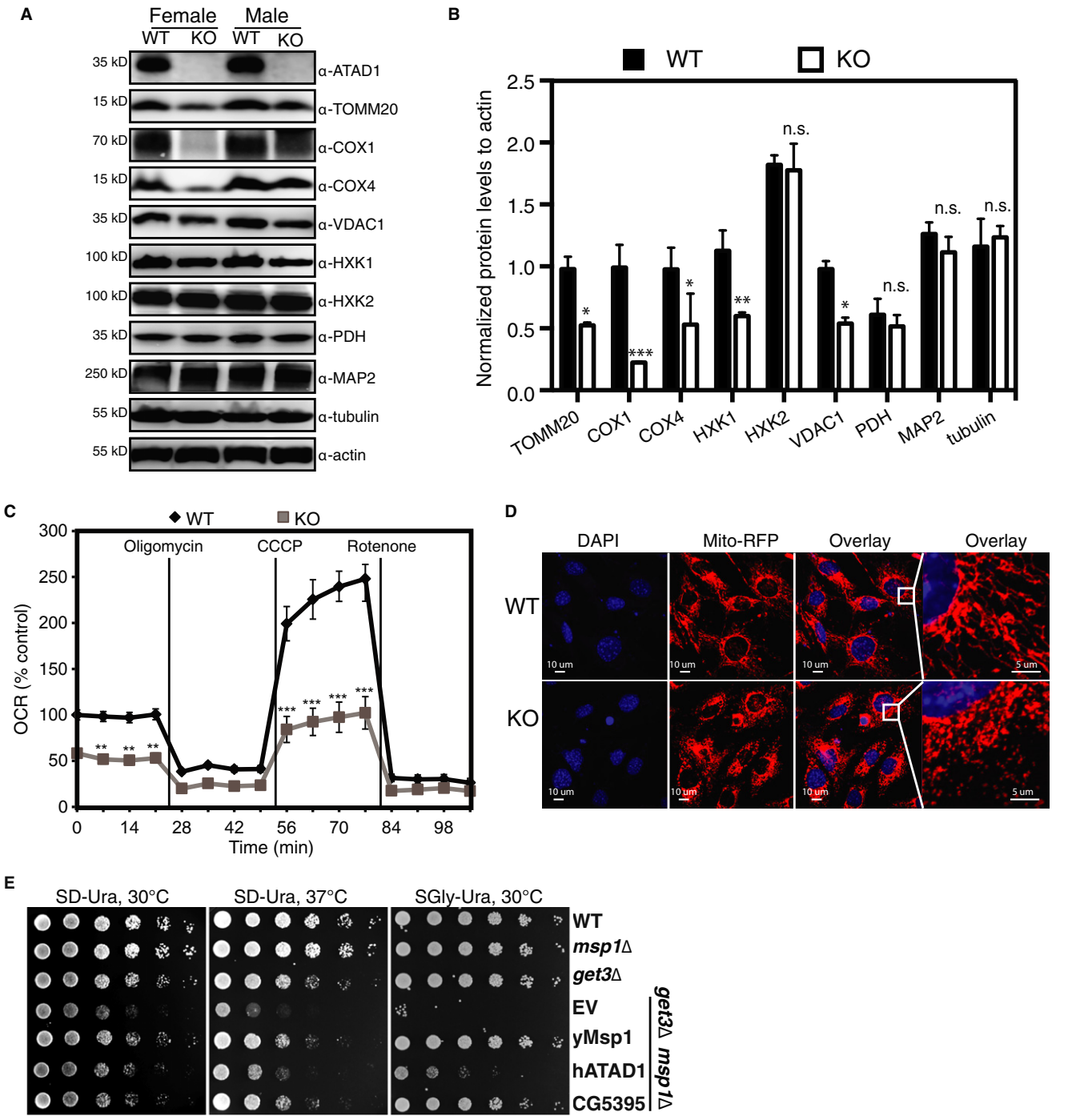

Figure 3. Depletion of *ATAD1* causes decreased mitochondrial protein level and mitochondrial fragmentation in mammals.

A Immunoblots of whole-brain lysates obtained from the wild-type (WT) and *ATAD1*$^{-/-}$ knockout (KO) mice. PDH, pyruvate dehydrogenase; HXK1 and 2, hexokinase 1 and 2.

B The optical densitometry quantification of (A). The values represent the mean ± SEM (n = 3, *P < 0.05, **P < 0.005, ***P < 0.001, one-way ANOVA, Tukey's multiple comparison tests).

C Oxygen consumption rate (OCR) of the WT and *ATAD1*$^{-/-}$ mouse embryonic fibroblasts (MEFs). The data were normalized to the amount of protein in each well and represent % control. **P < 0.005, ***P < 0.001.

D Representative images of the mitochondrial morphology of the WT and *ATAD1*$^{-/-}$ MEFs. The cells were transfected with Mito-RFP (red), stained with DAPI (blue), and visualized.

E Five-fold dilutions of the indicated strains harboring empty vector (EV), yeast Msp1, human ATAD1 or fly CG5395 construct cultured overnight in SD-Ura medium were spotted on SD-Ura or SGly-Ura plates and incubated at 30 or 37°C.

Source data are available online for this figure.

protein continues to be targeted to peroxisomes in the single-mutant strains (Supplementary Fig S4A). In the *get3*Δ *msp1*Δ mutant, we observed more complete co-localization of the GFP and RFP signals, which can only be seen with greatly extended exposure time due to the diminished mitochondrial content in this mutant (Fig 4A; see also Fig 2B and D). We also performed the converse experiment by overexpressing Msp1 in the *get3*Δ mutant expressing GFP-Pex15 and observed complete depletion of mislocalized Pex15 from the mitochondria (Fig 4B).

We tested the possibility that Msp1 binds and perhaps extracts mislocalized Pex15. Given that the wild-type Msp1 protein may associate with substrates transiently, we performed co-immunoprecipitation experiments using yeast strains expressing a 'substrate trap' E193Q mutant (asterisk in Fig 1A), which is predicted to bind substrates but fail to release them efficiently (Weibezahn *et al*, 2003; Hanson & Whiteheart, 2005). Consistent with this notion, exogenous expression of $Msp1^{E193Q}$ was unable to rescue the growth defect of the *get3*Δ *msp1*Δ mutant; moreover, it induced a dominant-negative phenotype in the *get3*Δ single mutant (Supplementary Fig S2B). As shown in Fig 4C, we observed that when Pex15 was overexpressed, it stably interacted with $Msp1^{E193}$ particularly in the *get4*Δ mutant background. Note that we consistently observed higher accumulation of $Msp1^{E193Q}$ in spite of it being expressed under the endogenous *MSP1* promoter. This possibly also contributes to the apparent interaction affinity relative to wild-type Msp1. It is also noteworthy that Pex15 exhibits elevated accumulation in the *get4*Δ mutant expressing the dominant-negative $Msp1^{E193Q}$, possibly related to mislocalization and stabilization on mitochondria (Fig 4C–input panel).

If the severe phenotype of the *get3*Δ *msp1*Δ double mutant is due to accumulation of mislocalized TA proteins in the mitochondrial outer membrane, overexpression of proteins like Pex15 should exacerbate this phenotype. To test this, we compared growth upon overexpression of GFP-Pex15 from the *GAL1* promoter. While the *get3*Δ *msp1*Δ mutant exhibited impaired growth on its own, the *GAL1::PEX15* construct caused a complete loss of growth on galactose medium (Fig 4D). One possible mechanism whereby Msp1 might maintain a low level of mislocalized TA proteins is to extract them and facilitate their degradation. We tested the half-life of GFP-Pex15 utilizing the stringent glucose repression of new transcription from the *GAL1* promoter. We first noticed that the steady-state level of Pex15 was increased in the *msp1*Δ mutant compared to WT (t = 0 min, Supplementary Fig S4B). Furthermore, the time-course of Pex15 degradation was significantly slower in the *msp1*Δ mutant (Supplementary Fig S4B and C) most likely due to impaired extraction and degradation of mitochondrial Pex15. To more rigorously test whether Msp1 limits mitochondrial Pex15 by facilitating its degradation, we measured the half-life of Pex15 in the *get3*Δ mutant expressing either the wild-type Msp1 or mutant $Msp1^{E193Q}$ (Fig 4E, Supplementary Fig S4D and E). Therefore, in both cases, Pex15 is strongly mislocalized to mitochondria (t = 0 min, Supplementary Fig S4D). Pex15 is significantly more stable in the strain expressing $Msp1^{E193Q}$ (Fig 4E and Supplementary Fig S4E). When we visualized the localization of GFP-Pex15 throughout the time-course, we observed that mitochondrial Pex15 was degraded faster in the *get3*Δ mutant expressing the wild-type Msp1 compared to the $Msp1^{E193Q}$, which still retained significant mitochondrial Pex15 after 180 min (Supplementary Fig S4D). Taken together, these results suggest that Msp1 is required to minimize the abundance of the Pex15 TA protein on mitochondria, most likely by promoting its extraction and degradation.

We also tested whether hATAD1 functions similarly to protect mammalian mitochondria from the mislocalization of PEX26, the human ortholog of Pex15. We established a human hepatocellular carcinoma (HepG2) cell line stably expressing GFP-PEX26 and repeatedly observed very modest mitochondrial GFP localization in a minority of cells (Fig 4F-top; marked by arrows). Knockdown of *ATAD1* with three distinct siRNAs (Fig 4G), however, greatly increased the overlap of GFP-PEX26 and Mitotracker Red (Fig 4F). We also observed that the overall intensity of the mitochondrial GFP signal was significantly enhanced, consistent with increased steady-state level of PEX26 in the whole-cell lysates from multiple cell lines (Fig 4F and Supplementary Fig S4F). Taken together, both yeast Msp1 and human ATAD1 protein are important to minimize the mitochondrial mislocalization of the TA proteins, Pex15, and PEX26, respectively.

Figure 4. Yeast Msp1 and human ATAD1 are required to limit the level of mitochondrially mislocalized TA proteins Pex15 and PEX26, respectively.

A Representative images of GFP-Pex15 localization. The indicated yeast strains expressing GFP-Pex15 from the *GAL1* promoter and plasmid-borne Mito-RFP were grown overnight in SD medium, switched to galactose induction medium for 6 h, and visualized by fluorescence microscopy. The *get3*Δ *msp1*Δ images (1,000 ms) were exposed 5 times longer than the WT, *msp1*Δ, and *get3*Δ images (200 ms).

B The WT and *get3*Δ strain expressing GFP-Pex15 from the *GAL1* promoter and the plasmid-borne Mito-RFP were transformed with either EV or a Msp1 overexpressing construct ($Msp1_{(2\mu)}$) and subjected to the same procedure as described in (A).

C Pex15 co-immunoprecipitates with the 'trap mutant' $Msp1^{E193Q}$. Msp1 was immunoprecipitated by anti-HA antibodies from digitonin-solubilized mitochondria that were extracted from the indicated strains overexpressing GFP-Pex15 from the *GAL1* promoter and empty vector (–), wild-type Msp1 (WT) or $Msp1^{E193Q}$ (E193Q). Pex15 expression was induced in galactose medium for 6 h. 4% of the crude lysates, and final eluates were immunoblotted with anti-HA and GFP. Om45 is a mitochondrial outer membrane protein and is used as a loading control.

D Five-fold dilutions of the indicated strains expressing Pex15 from the native *PEX15* promoter or *GAL1* promoter (P_{GAL1}::*GFP–PEX15*) were grown overnight in SD medium, spotted on SD or synthetic galactose (SGal) plates, and cultured at 30°C.

E The *get3*Δ strain co-expressing GFP-Pex15 from the *GAL1* promoter and wild-type Msp1 or $Msp1^{E193Q}$ was pulsed in galactose medium for 5 h to induce GFP-Pex15 accumulation and chased in glucose medium to shut off transcription. Whole-cell lysates were prepared from cells harvested every 45 min and analyzed by immunoblot. Por1 is the loading control.

F HepG2 cells stably expressing GFP-PEX26 were treated with scrambled siRNA (scr) or siRNAs (#1–3) targeting human *ATAD1* for 6 days, stained with Mitotracker Red, and visualized by fluorescence microscopy with equivalent exposure times.

G Whole-cell lysates of cells from (F) were analyzed by immunoblot using the indicated antibodies. QCR2 is a mitochondrial protein and is used as a loading control.

Source data are available online for this figure.

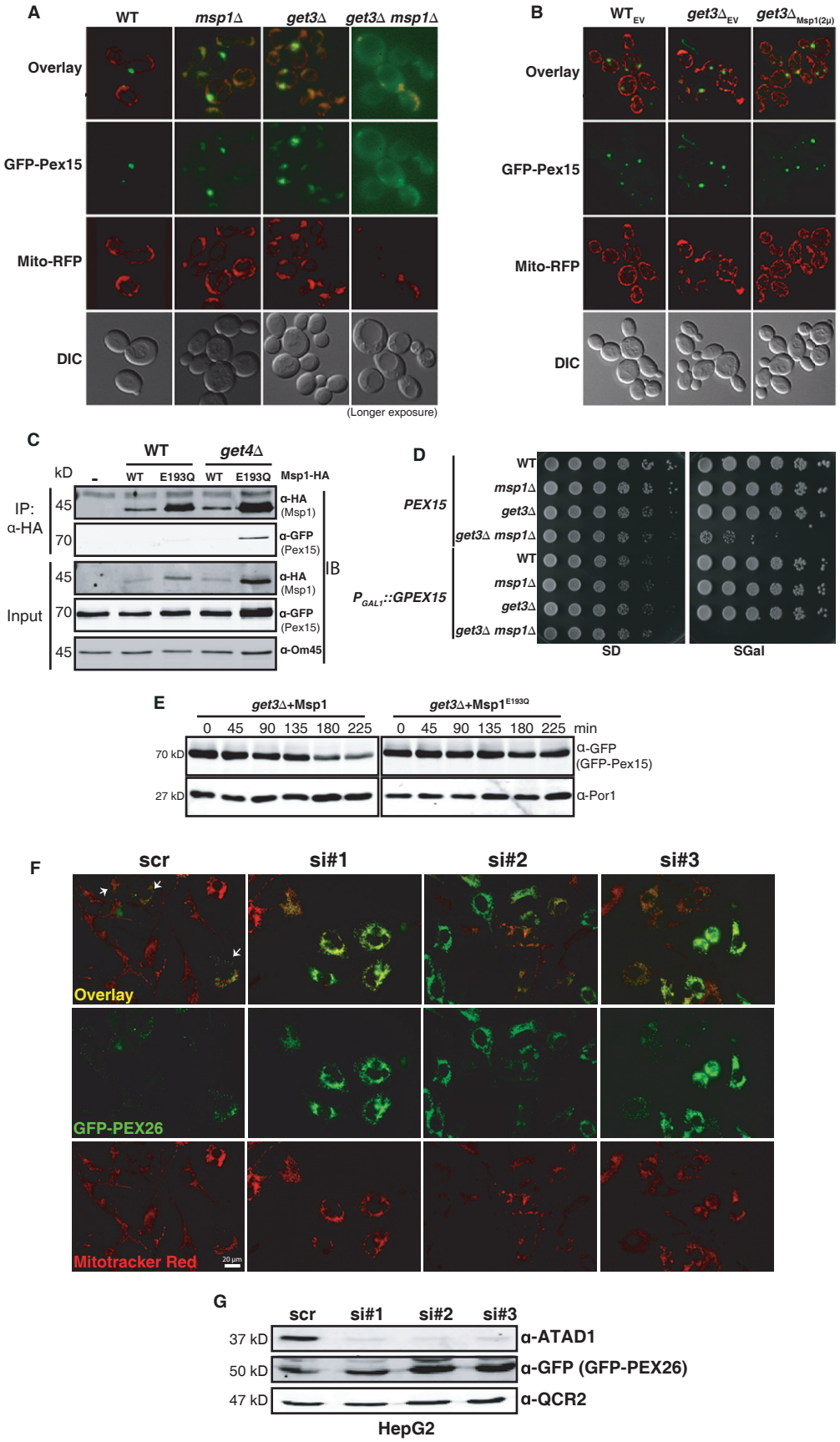

Figure 5. Msp1 physically interacts with the TA protein Gos1 and is required to limit mitochondrial Gos1.

A Gos1 co-immunoprecipitates with the 'trap mutant' Msp1. Msp1 was immunoprecipitated by anti-HA antibody from digotonin-solubilized mitochondria that were extracted from the indicated strains expressing GFP-Gos1 from the native *GOS1* promoter and empty vector (−), wild-type Msp1 (+) or Msp1^{E193Q} (E193Q). 4% of the crude lysates and final eluates were immunoblotted with anti-HA, GFP, and Om45 antibodies. Om45 is a control mitochondrial outer membrane protein.

B The indicated strains expressing GFP-Gos1 from the native promoter and Mito-RFP were grown in SD medium to early log phase and visualized by fluorescence microscopy.

C The *get3*Δ strain expressing GFP-Gos1 from the *GAL1* promoter was transformed with EV or Msp1^{E193Q}, grown in galactose medium for 5 h to induce Gos1 expression and then switched to glucose medium to shut off transcription. Cells were harvested every 30 min thereafter, and the whole-cell lysates were analyzed by immunoblot.

D Representative images of the *GAL1* promoter-based transcriptional shut-off experiment as described in (C) except that the indicated strains were co-transformed with Mito-RFP to visualize mitochondria.

E Five-fold dilutions of the indicated strains harboring either empty vector (−) or Gos1 overexpression 2 μ vector (+) were spotted on SD or SGly plates and incubated at 30 or 37°C.

Source data are available online for this figure.

Msp1/hATAD1 physically interacts with and is required to prevent TA protein Gos1/GOS28 misaccumulation on mitochondria

To identify *bona fide* substrates of Msp1, we performed a two-step purification using a yeast strain expressing Msp1-His$_6$/HA$_3$ tag from the *MSP1* promoter. We expressed the wild-type or E193Q mutant Msp1 in both the WT and *get3*Δ strains and purified Msp1 by two-step purification. In examining potential substrates, we aimed to look for proteins that fulfill two criteria. First, they are purified more efficiently by the 'trap mutant' Msp1^{E193Q} than by the wild-type protein. Second, they exhibit stronger association with Msp1 in the *get3*Δ mutant strain than in the WT strain. As shown in Supplementary Table S1, Gos1 meets both criteria and is one of the most abundant proteins detected by mass spectrometry. Importantly, it is also a TA protein and functions as a v-SNARE in Golgi vesicular trafficking (McNew *et al*, 1998). We first verified this result by conducting a directed co-immunoprecipitation experiment. We expressed GFP-Gos1 and Msp1-HA fusion proteins under their endogenous promoters and performed an anti-HA immunoprecipitation from crude mitochondrial lysate. As seen in Fig 5A, GFP-Gos1 showed a stable association with Msp1^{E193Q}. We also observed a stronger GFP-Gos1 purification with Msp1^{E193Q} in the *get3*Δ and *get4*Δ mutants compared to a strain with a functional GET system (WT). Note that Msp1^{E193Q} consistently accumulated at a higher level compared to the wild-type protein (Fig 5A – input panel; also see Fig 4C – input panel). Similar to Pex15, the steady-state level of Gos1 was higher in the *get3*Δ and *get4*Δ mutant strains expressing the dominant-negative Msp1^{E193Q} mutant (Input panel, Fig 5A). To test Gos1 localization, we expressed GFP-Gos1 under the endogenous *GOS1* promoter and observed a partial overlap of GFP-Gos1 signal with Mito-RFP in both the *get4*Δ *msp1*Δ mutant strain and in the *get3*Δ mutant expressing the dominant-negative Msp1^{E193Q} (Fig 5B and Supplementary Fig S5A).

To test whether Msp1 facilitates the degradation of mislocalized Gos1, we used the *GAL1* promoter-based transcriptional shut-off system to test its half-life. Overexpression of Gos1 from the *GAL1* promoter leads to its mislocalization to the mitochondria of the *get3*Δ mutant (T = 0 min, Fig 5D). The time-course of Gos1 degradation in the *get3*Δ mutant expressing dominant-negative Msp1^{E193Q} is significantly slower than the *get3*Δ mutant, which expresses endogenous wild-type Msp1 (Fig 5C). We also visualized the localization of GFP-Gos1 throughout the time course. We observed that mitochondrial Gos1 was degraded faster in the *get4*Δ mutant compared to the strain expressing Msp1^{E193Q}, which still retained significant mitochondrial Gos1 after 180 min (Fig 5D).

To further address whether misaccumulation of Gos1 contributes to the mitochondrial damage in the *get3*Δ *msp1*Δ mutant, we attempted to delete *GOS1* and test for rescue of the growth phenotype. Unfortunately, loss of Gos1 in our W303-1a strain background causes lethality (Supplementary Fig S5B). Instead, we reasoned that overexpression of Gos1 might overload mitochondria and exacerbate the growth phenotype caused by loss of Msp1 and/or the GET system. As shown in Fig 5E, overexpression of Gos1 either caused or exacerbated growth phenotypes in *get1*Δ, *get2*Δ, and *get3*Δ single mutants. The double mutants containing those deletions combined with an *msp1*Δ mutation already exhibited such severe growth defects that Gos1 had no additional consequence. However, the *get4*Δ *msp1*Δ, *get5*Δ *msp1*Δ, and *msp1*Δ *sgt2*Δ double mutants, which maintained much more mitochondrial function (See Fig 2), were markedly impaired by Gos1 overexpression, particularly in glycerol growth (Fig 5E). The effect of Gos1 overexpression is specific as overexpression of Sbh1, an endoplasmic reticulum TA protein that does not mislocalize to mitochondria, did not exacerbate the growth phenotypes (Supplementary Fig S5C) (Schuldiner *et al*, 2008).

In addition to Gos1, we also observed that Tom5, a native mitochondrial TA protein, was strongly purified by Msp1^{E193Q} in the wild-type and the *get3*Δ mutant strain (Supplementary Table S1). This observation raised the possibility that Msp1 might not only bind to non-native, mislocalized mitochondrial TA proteins but also to native proteins. To test this hypothesis, we tagged Tom5 and all other mitochondrial TA proteins, Tom6, Tom7, Tom22, Fis1, Gem, and Fmp32 with a GFP at their N-termini and performed co-immunoprecipitation experiments (Supplementary Fig S6A). We observed no interaction between Tom5, Tom6, Fis1, Gem1, or Fmp32 and either wild-type Msp1 or the Msp1^{E193Q} mutant. Tom7 and Tom22 showed an interaction, but it was with both the wild-type and mutant Msp1 protein. More importantly, we observed no significant delay in the rate of degradation of any of these native mitochondrial TA proteins in the *msp1*Δ mutant (Supplementary Fig S6B). Furthermore, overexpression of *TOM5*, *TOM6*, or *TOM7* did not exacerbate the growth phenotype of the *msp1*Δ mutant strain (Supplementary Fig S6C). Therefore, it appears that none of the native mitochondrial TA proteins are efficient substrates of Msp1, at least in the conditions in which we conducted these experiments.

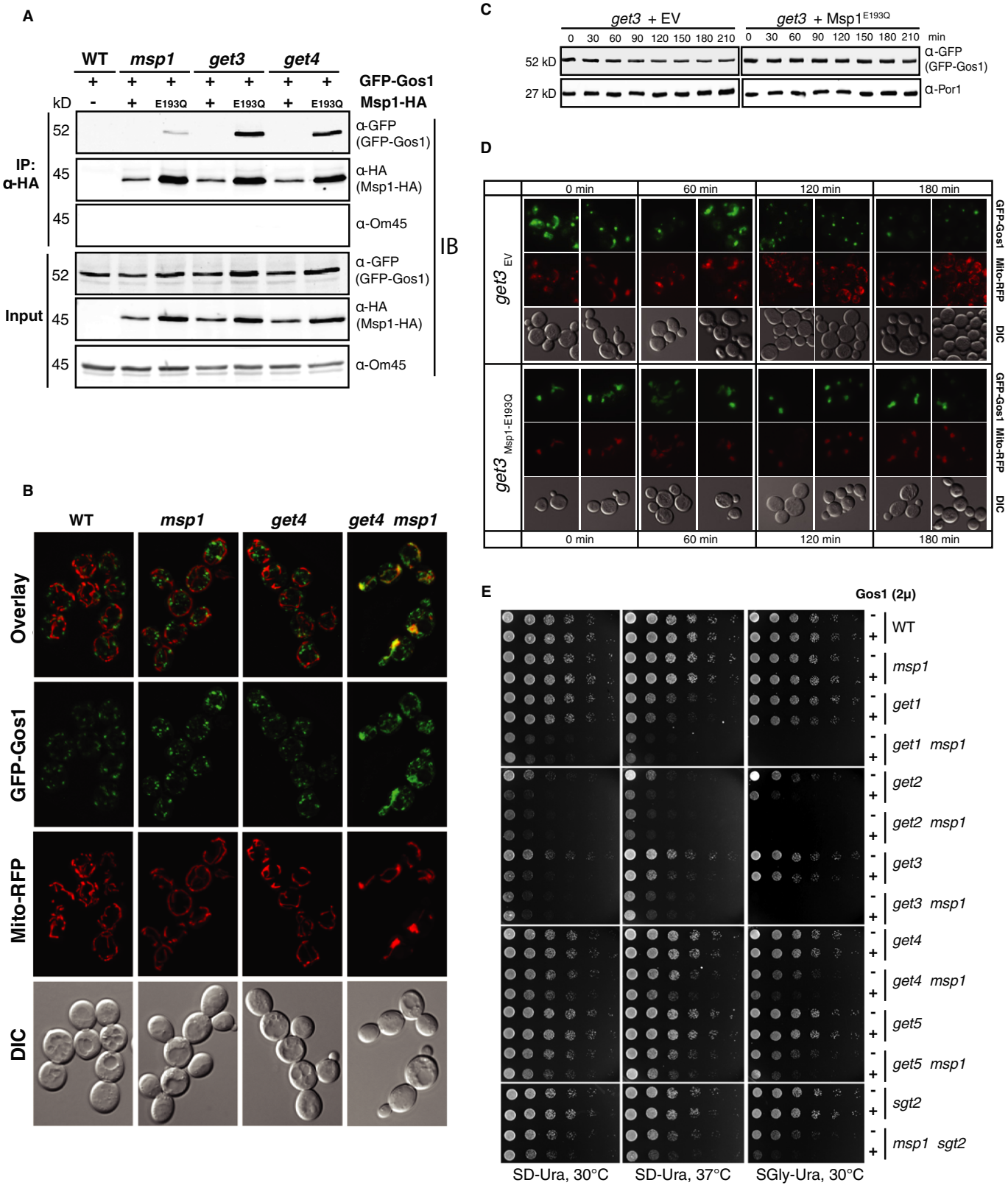

Based on our observations with Gos1, we performed two experiments to test whether GOS28, the mammalian ortholog of yeast Gos1, is subjected to mitochondrial misaccumulation, which is prevented by ATAD1. First, to test whether GOS28 misaccumulates on mitochondria upon ATAD1 depletion, we established a human dermal fibroblast (HDF) cell line stably expressing a GFP-human

GOS28 fusion protein and subjected it to knockdown with control and *ATAD1* siRNAs. In control siRNA (scr)-treated cells or cells treated with si#4 that fails to knockdown *ATAD1* (Fig 6B), the majority of the GFP signal was localized to the peri-nuclear Golgi apparatus and had no overlap with Mitotracker Red (Fig 6A). However, when *ATAD1* was knocked down by si#1, 2, or 3 (Fig 6B), we clearly observed a partial redistribution of GFP-GOS28 to overlap with Mitotracker Red (Fig 6A). Second, to directly test whether GOS28 physically interacts with ATAD1, we assessed co-immunoprecipitation using crude mitochondrial extract from HepG2 cells stably expressing GFP-GOS28 and empty vector, wild-type ATAD1 or a substrate trap mutant ATAD1 ($ATAD1^{E193Q}$). Only the $ATAD1^{E193Q}$ mutant purified detectable amounts of GOS28 (Fig 6C). Note that the steady-state GOS28 level was reproducibly elevated in cells expressing the $ATAD1^{E193Q}$ (Fig 6C, lane 3), which is likely caused by its dominant-negative activity. This is consistent with the observation that expression of $ATAD1^{E193Q}$ causes ectopic accumulation of GFP-GOS28 on the mitochondria (Supplementary Fig S7A). Most importantly, we further observed increased steady-state abundance of endogenous GOS28 in multiple $ATAD1^{-/-}$ mouse tissues, including brain, liver, and heart (Fig 6D and Supplementary Fig S7B). We therefore conclude that Gos1 and GOS28 are *bona fide* substrates of yeast Msp1 and mammalian ATAD1, respectively.

Discussion

Based on the data presented herein, we conclude that yeast Msp1 and human ATAD1 belong to an evolutionarily and functionally conserved protein family. We demonstrate that they play a role in quality control of mitochondrial outer membrane proteins. Specifically, Msp1 or ATAD1 prevents a subset of TA proteins (yeast–Pex15 and Gos1; mammals–PEX26 and GOS28) that escape from the GET or TRC system from inappropriately accumulating on the mitochondria, likely by extracting them and facilitating their cytoplasmic degradation. The physiological consequences of combined impairment of Msp1 and the GET system include loss of mtDNA, loss of mitochondrial resident proteins, and severely altered mitochondrial morphology. The principal evidence supporting this model is enumerated below.

First, we have found that the targeting and insertion systems for TA proteins are quite imprecise. This necessitates quality control systems to manage the burden of TA proteins that are mislocalized to other cellular compartments. In mammals, the cytoplasmic Bag6 protein not only participates in chaperoning TA proteins to the ER for insertion, but also mediates ubiquitination of proteins that are inappropriately released from ribosomes (Mariappan *et al*, 2010; Hessa *et al*, 2011). We suggest that the Msp1 protein family represents a similar protein quality control system for the mitochondria. This system is necessitated by the fact that, even when the GET or TRC system is fully functional, TA proteins can escape and mislocalize to mitochondria. This is demonstrated by our observation that deletion of Msp1 alone caused ectopic accumulation of Pex15 protein on yeast mitochondria (Fig 4A). This is also true for both PEX26 and GOS28 when ATAD1 protein was depleted in multiple human cell lines (Figs 4G and 6A and Supplementary Fig S7A). For reasons that remain unclear, the mitochondrial membrane appears to be a receptive host for TA proteins that fail to target their native membrane. It is possible that this is because the mitochondrial outer membrane appears to be one of the only two organelles where TA proteins are directly targeted and inserted. Previous reports and our data (Fig 4A) clearly show that genetic impairment of the GET system causes mislocalization of a subset of TA proteins on the mitochondria (Schuldiner *et al*, 2008; Jonikas *et al*, 2009). Therefore, we suggest that cells have evolved a protein quality control system residing on mitochondria to handle this burden of mislocalized TA proteins.

Second, Msp1 physically interacts with mislocalized TA proteins. Our two-step purification identified the TA protein Gos1 as a possible genuine substrate of Msp1, which interacts with the substrate trap mutant Msp1 (Supplementary Table S1 and Fig 5A). This Msp1 mutant can also stably bind to overexpressed Pex15, but for unknown reasons, we did not observe Pex15 in the Msp1 co-purification experiment. Presumably, the substrate trap mutant Msp1 stabilizes the physical interaction with substrates, while wild-type Msp1 may bind to them transiently. It is also possible, however, that the enhanced observed binding of mutant Msp1 is simply a function of its elevated accumulation. Beyond Gos1 and Pex15, we expect that additional substrates remain to be discovered. Interestingly, we also identified Tom5 as another potential substrate by Msp1 co-purification; however, we failed to recapitulate this result using directed co-immunoprecipitation experiments (Supplementary Fig S6A). It is possible that the observation of co-purification is an artifact, and Tom5 and Msp1 have no relationship. It is also possible, however, that Tom5 is a *bona fide* substrate of Msp1, but we failed to obtain evidence for this either due to the specific conditions of our experiments or the use of a GFP-Tom5 fusion protein. As a result, we do not firmly conclude that Msp1 cannot recognize native mitochondrial TA proteins as substrates. In addition, it is possible that Msp1 extracts a broader range of protein substrates, including non-TA proteins, which is consistent with our observation of non-TA mitochondrial proteins bound specifically to the Msp1-E193Q mutant in the two-step purification experiment (Supplementary Table S1). In fact, mammalian ATAD1 (possibly the cytoplasmic pool) was shown to extract or disassemble the AMPAR protein complex, which has no TA protein constituents, from the cell surface (Zhang *et al*, 2011). Therefore, while Msp1/ATAD1 clearly functions in the degradation of mitochondrially mislocalized TA proteins, it appears to function in a broader context as well.

Third, Msp1 is required for the normal rate of degradation of mislocalized TA proteins. We repeatedly observed that the steady-state level of Msp1 substrate proteins is higher in Msp1- or ATAD1-depleted cells. Furthermore, we conducted a chase experiment on Pex15 and Gos1 and demonstrated that their half-life is extended in the absence of Msp1 (Fig 4E, Supplementary Figs S4B–E and S5C and D). We speculate that Msp1 unfolds and extracts Pex15 and Gos1 via ATP hydrolysis by the AAA+ domain. However, unlike *m*- or *i*-AAA ATPase, which has an accessory proteolytic domain to digest the unfolded peptide, Msp1 possesses only the AAA+ domain. Therefore, the mechanisms whereby mislocalized TA proteins are degraded in the cytosol remain to be explored. It is known that the cytoplasmic proteasome is engaged to degrade membrane proteins from various organelles, including the ER and mitochondria (Neutzner *et al*, 2007; Karbowski & Youle, 2011; Taylor & Rutter, 2011). Therefore, it seems likely that proteasomes provide the major degradative activity for TA proteins once they are extracted from the mitochondria.

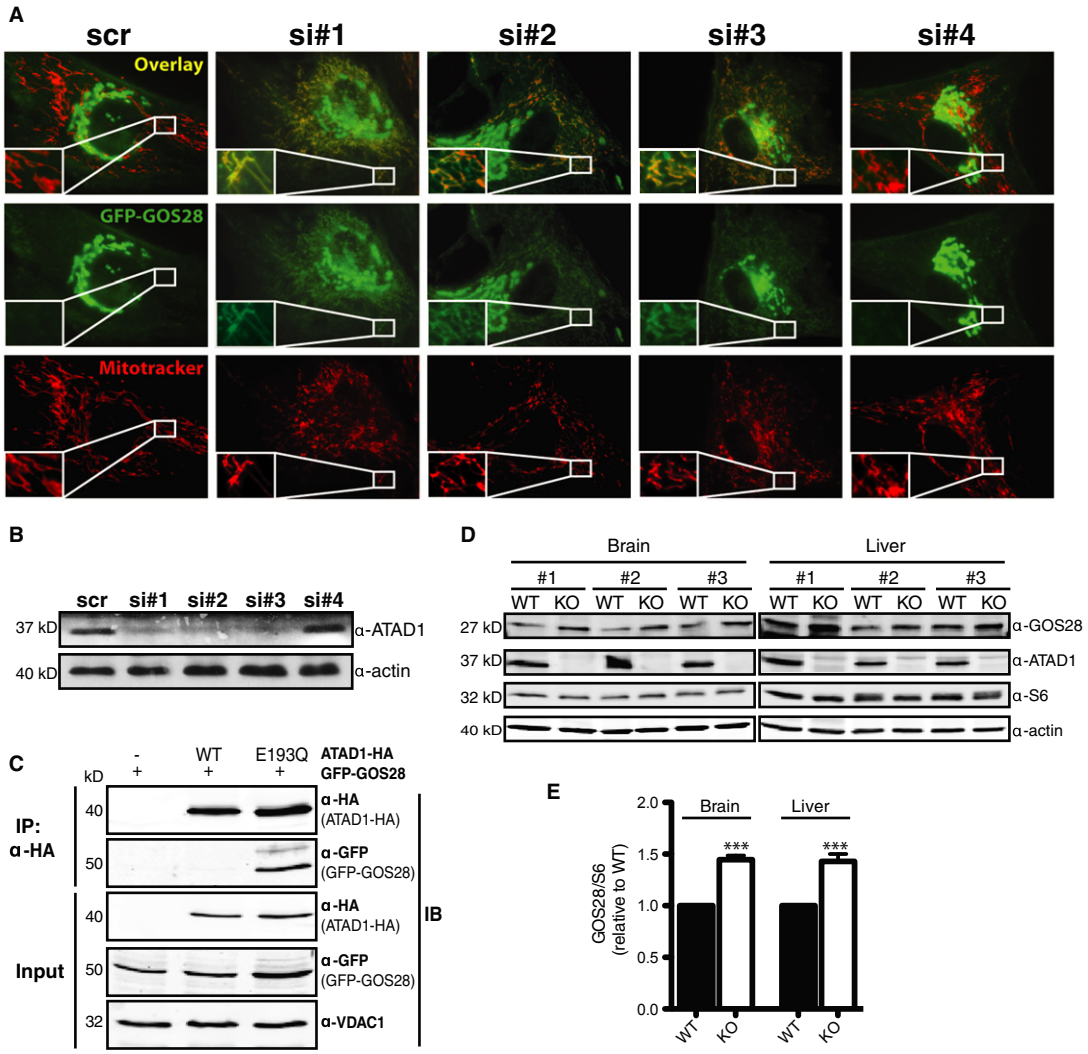

Figure 6. ATAD1 physically interacts with the TA protein, GOS28, and is required to limit the level of mislocalized GOS28 on mitochondria in mammals.

A Human dermal fibroblasts (HDFs) stably expressing GFP-GOS28 were treated with scr or siRNA (#1-4) against h*ATAD1*, stained with Mitotracker Red, and visualized by fluorescence microscopy.

B Whole-cell lysate of cells from (A) were immunoblotted using anti-ATAD1 and actin (loading control) antibodies.

C Crude mitochondria were extracted from HepG2 cells that stably co-express GFP-GOS28 with empty vector (–), HA-tagged wild-type ATAD1 (WT), or ATAD1^{E193Q} mutant. ATAD1 was immunoprecipitated using anti-HA antibody from digitonin-solubilized lysates and 5% of the crude lysates, and eluates were immunoblotted with anti-GFP and HA antibodies.

D Mouse tissue lysates (30 μg protein) from three WT and *ATAD1*$^{-/-}$ mice were analyzed by immunoblot. S6 ribosomal protein and actin are used as loading controls.

E The optical densitometry quantification of (D). The values represent the mean ± SEM (***$P < 0.001$, one-way ANOVA).

Source data are available online for this figure.

Fourth, the Msp1 and ATAD1 proteins are essential for the maintenance of mitochondria. We observed that loss of both Msp1 and the GET system causes loss of mtDNA and protein, and severe morphological defects (Fig 2). Mammalian cells, however, seem to be more susceptible to the depletion of ATAD1 as mutation of ATAD1 is sufficient to cause significant mitochondrial impairment (Fig 3A–D). Prior to this study, the major connection between the GET system and mitochondria related to TA protein mislocalization to mitochondria upon GET system disruption. Perhaps, the most profound mitochondrial defect observed is the loss of mitochondrial protein content in the *get1*Δ *msp1*Δ, *get2*Δ *msp1*Δ, and *get3*Δ *msp1*Δ mutant strains, which cannot be explained by the loss of mtDNA. Given that the TA proteins Tom5, Tom6, Tom7, and Tom22 are critical components of the TOM complex, perhaps ectopic TA protein accumulation causes defects in TOM complex formation. The ectopic TA proteins could either displace one or more of the tail-anchored components of the TOM complex, rendering it inactive. Alternatively, hyper-accumulation of TA proteins could impair the unknown mitochondrial TA protein import system, leading to decreased import efficiency of Tom5, Tom6, Tom7 and/or Tom22 and therefore impaired mitochondrial protein import. We also observed altered mitochondrial morphology in both *msp1*Δ yeast and *ATAD1* knockdown cells. Intriguingly, before the function of the GET system was determined, Get1 (also known as Mdm39) was

discovered in a genetic screen for genes important for mitochondrial distribution and morphology (Dimmer *et al*, 2002). Perhaps, this observation relates to the effect of mislocalized TA proteins, caused by mutation of *GET1*, to impair mitochondrial morphology. In fact, many mitochondrial shaping factors such as Fis1 (yeast and mammals), Mff (mammals), and Gem1 (yeast) are TA proteins. Therefore, as speculated for the TOM complex above, mitochondrial morphology and dynamics might be susceptible to aberrant accumulation of non-mitochondrial TA proteins. For example, mislocalization of the Gos1 v-SNARE protein might enable promiscuous fusion events with organelles displaying cognate t-SNARE proteins.

Finally, our data suggest that the mitochondrial function of Msp1 protein family is conserved between yeast, flies, and mammals. Both *Drosophila CG5395* and human *ATAD1* suppressed the respiratory growth phenotype of the *get3*Δ *msp1*Δ mutant strains (Fig 3E). In addition, depletion of ATAD1 caused accumulation and mitochondrial localization of PEX26 and GOS28 as well as mitochondrial defects (Figs 3, 4G and 6, and Supplementary Fig S3D). In *Drosophila*, mitochondria undergo dramatic morphological changes during spermatogenesis. At the onion stage, mitochondria form a specialized structure called the nebenkern (Tokuyasu, 1975). Mutation of the fly *MSP1* ortholog *CG5395* (*nmd* mutant, *no mitochondrial derivative*) leads to a much smaller nebenkern and a slight loss of mitochondrial membrane potential (Noguchi *et al*, 2011). While these data do not implicate impaired protein quality control, it demonstrates that this gene is important in mitochondrial morphology and function. Furthermore, *ATAD1* knockout mice exhibit severe neuronal defects, including deficiencies in learning and memory and a seizure-like syndrome (postnatal day 19–25) (Zhang *et al*, 2011). Interestingly, we observed ectopic accumulation of GOS28 in multiple tissues from *ATAD1*$^{-/-}$ mice, particularly the brain (Fig 6D). Some of these neuronal deficits are likely due to the failure of disassembly of the AMPAR receptor, but similar neuronal phenotypes are observed with impaired mitochondrial quality control in mice and humans (Rugarli & Langer, 2012). We speculate that the mitochondrial defects caused by loss of *ATAD1* might partially contribute to the phenotype of the *ATAD1*$^{-/-}$ mice.

In conclusion, we suggest that the Msp1/ATAD1 protein family performs an evolutionarily conserved role in quality control of the mitochondrial outer membrane. This function, while perhaps including additional activities, is likely to extract and promote the degradation of TA proteins that have been mislocalized to mitochondria. The consequences for failure of this activity, particularly under a stress to the GET system, are devastating for mitochondrial morphology and function. Given the critical importance of mitochondrial quality control in human physiology and pathophysiology, we anxiously await a broader and deeper understanding of this protein family in health and disease.

Materials and Methods

Yeast strains and growth conditions

Saccharomyces cerevisiae W303-1a (*MATa, his3 leu2 met15 trp1 ura3*) was used in this study. The standard PCR-based homologous recombination method was used to generate all mutant strains. Briefly, drug selection cassette (KanMX4, hphMX4, or natMX4) flanked with 45-bp fragments upstream and downstream of the gene of interest was PCR amplified and transformed into the wild-type diploid (Goldstein & McCusker, 1999) (Wach *et al*, 1994). The haploid strain was generated by sporulation and tetrad analysis. The strains with chromosomally integrated P_{GAL1}-*GFP-PEX15* were generated as described in (Longtine *et al*, 1998). The genotype of the strain was verified by standard genotyping PCR. The genotypes of all yeast strains used in this study are listed in Supplementary Table S2.

For yeast transformation, the standard lithium acetate procedure was used (Gietz *et al*, 1992). Transformed yeast cells were grown in synthetic complete dextrose (SD) medium lacking the appropriate amino acid(s) for auxotrophic selection purposes at 30°C. Media used in this study include standard YP and synthetic minimal medium supplemented with 2% glucose, 2% raffinose, or 3% glycerol. Solid plates contain 2.2% (w/v) agar.

Plasmid construction

To produce plasmids expressing non-tagged, C-terminal His_6/HA_3 or GFP-tagged Msp1, the *MSP1* ORF flanked with its upstream 500-bp promoter region was PCR amplified from yeast genomic DNA and ligated into the pRS416, pRS426, or pRS416 vector containing either a C-terminal His_6/HA_3 or GFP tag. Msp1^{E193Q} construct was made by site-directed mutagenesis of the Msp1-His_6/HA_3 construct. To generate human *ATAD1* and fly *CG5393* constructs, *ATAD1* and *CG5393* ORF were amplified from HepG2 and fly cDNA, respectively, and ligated into pRS416-based vector containing the *ADH1* promoter (Mumberg *et al*, 1995). N-terminal GFP-tagged Gos1 construct was made by ligating P_{GOS1}, *GFP*, and *GOS1* ORF fragments together using the standard sewing PCR and ligating into the pRS414 vector. The P_{GAL1}::GFP-Gos1 construct was generated by ligating *GOS1* ORF into pRS414-based vector containing the *GAL1* promoter and a N-terminal GFP tag. The Retro-X^{TM}Q Vectors (Clontech) were used to generate mammalian constructs. Human *ATAD1* ORF fused with HA or GFP tag at the 3′-end or *PEX26* or *GOS28* ORF fused with GFP at the 5′-end was ligated into pQCXIP or pQCXIZ vector. Site-directed mutagenesis was used to convert ATAD1-HA into ATAD1^{E193Q}-HA. Peroxisomal fluorescent marker construct was made by fusing RFP protein with the peroxisomal targeting sequence (SKL) at the C-terminus.

Isolation of yeast mitochondria

Yeast cells were harvested at mid-log phase (OD_{600} = 2–3) unless indicated otherwise. Preparation of crude and purified mitochondria was as described previously (Boldogh & Pon, 2007). Yeast pellet was washed once with ddH_2O, resuspended, and incubated in TD buffer (100 mM Tris-SO_4, pH 9.4 and 100 mM DTT) for 15 min at 30°C. Spheroplasts were obtained by incubating cells in SP buffer (1.2 M sorbitol and 20 mM potassium phosphate, pH 7.4) supplemented with lyticase (2 mg/g of cell pellet) (Sigma-Aldrich) for 1 h at 30°C to digest the cell wall. Spheroplasts were gently washed once in ice-cold SHE buffer (1.2 M sorbitol, 20 mM HEPES-KOH, pH 7.4, 2 mM $MgCl_2$, 1 mM EGTA, and 1 mM PMSF) and homogenized in ice-cold SHE buffer that contains 0.6 M sorbitol with a Dounce homogenizer applied with 10-20 strokes. The crude mitochondrial fraction was obtained by differential centrifugation. Protein concentration was determined using Bradford protein assay (Bio-Rad).

Continuous Nycodenz gradients were used to purify crude mitochondria. To make a gradient, 2.1 ml of 5, 10, 15, 20, and 25% Nycodenz in SHE buffer was layered in 14 × 89 mm Ultra-Clear centrifuge tubes (Beckman) and the tubes were sat at room temperature for 3–4 h to allow the Nycodenz to diffuse. Crude mitochondria were loaded on top of the chilled gradient and separated at 100,000 × *g* for 1 h at 4°C (SW41 rotor; Beckman). Intact purified mitochondria were recovered from a brown band at around 16% Nycodenz concentration.

Assessment of sub-mitochondrial localization

The experiment was conducted as described previously (Chen *et al*, 2012). Briefly, proteinase-free mitochondria were incubated in the isotonic SH buffer (0.6 M Sorbitol, 20 mM HEPES-KOH) or hypotonic H buffer (20 mM HEPES-KOH) with and without 1% Triton X-100. Proteinase K (10 μg/μl) was then added and incubated on ice for 20–30 min. The digestion was stopped by adding phenylmethylsulfonyl fluoride (PMSF) to 2 mM. The reaction mixtures were denatured in 6× Laemmli buffer and resolved by 12% SDS-PAGE, followed by immunoblot.

The high-salt and alkaline extraction were adapted from a previously described protocol (Boldogh & Pon, 2007). Intact mitochondria were treated with salt (100 mM KCl in SHE buffer without sorbitol) or carbonate (100 mM Na_2CO_3 in SHE buffer) for 30 min on ice and subjected to ultracentrifugation (100,000 × *g* for 20 min) to separate soluble and insoluble proteins. Soluble fractions were precipitated by 15% trichloroacetic acid (TCA) and dissolved in 1× Laemmli buffer. An equal amount of lysate from both the soluble and insoluble fraction was analyzed by immunoblot.

Two-step Msp1-His_6/HA_3 purification

Crude mitochondria isolated from strains grown in synthetic raffinose medium to mid-log phase (OD_{600} = 2.5) were solubilized in lysis buffer (20 mM HEPES, pH 7.4, 10 mM KCl, 1.5 mM $MgCl_2$, 1 mM EDTA, 150 mM NaCl, 10 mM imidazole, 2.1 mg/ml NaF, 10.8 mg/ml 2-glycerolphosphate, 0.5% digitonin and protease inhibitors) for 1 h at 4°C. For the first step of the purification, cleared mitochondria lysates were incubated with equilibrated Ni-NTA beads for 1 h at 4°C. Ni-NTA beads were washed 5 times with wash buffer (compositions are same as lysis buffer except for 20 mM imidazole and 0.05% digitonin). Proteins were eluted three times by 250 mM imidazole under non-denaturing conditions. For the second step of the purification, final eluates of the first purification were combined and mixed with anti-HA antibody-conjugated agarose (A2095; Sigma) for 1 h at 4°C. The agarose was then washed five times, and proteins were eluted five consecutive times by 1 mg/ml HA peptides. Final eluates were precipitated in 15% TCA overnight at 4°C and analyzed by mass spectrometry.

Fluorescence microscopy

Yeast samples were prepared by growing yeast cells to early log phase (OD_{600} = 0.8–1) in synthetic dropout medium with appropriate carbon sources at 30°C. To prepare mammalian cell samples, we cultured cells on Poly-L-Lysine-coated Lab-Tek II chamber slides for a day to allow them to fully attach. They were either visualized directly or stained with 25 nM Mitotracker Red CMXRos (Life Technologies) in FBS-free medium for 5 min at 37°C before imaged. To examine morphological changes in mitochondria from *ATAD1*$^{-/-}$ MEFs, they were transiently transfected with Mito-RFP to label the mitochondria. Transfected cells were fixed for 15 min with 4% PFA + 4% sucrose in PBS without permeabilization. Cells were washed three times with PBS buffer, stained with DAPI, and washed three more times with PBS buffer. Images of the cells were acquired by using a Zeiss LSM 710 laser-scanning confocal microscope using a 40× oil-immersion objective.

Cells were imaged on the Axio Observer. Z1 imaging system (Carl Zeiss) equipped with 40× and 100× objectives (oil-immersion). Digital fluorescence and differential interference contrast (DIC) images were acquired using a monochrome digital camera (AxioCam MRm, Carl Zeiss). *Z*-stacks of 0.35-μm slides were obtained and deconvolved using the AxioVision software (Version 4.8, Carl Zeiss). 2D projection of the *z*-stacks was performed using the ImageJ software. The final images were adjusted and assembled using Adobe Photoshop CS5.1. Brightness and contrast were adjusted only using linear operation on the entire image.

The yeast fluorescent images shown in this study are representative pictures from at least two independent experiments ($n \geq 2$). The images of the mammalian cells are representative of three independent experiments ($n = 3$).

Mass spectrometry

TCA pellets were resuspended in 8 M urea, 50 mM HEPES, and pH 8.8. Proteins were reduced by the addition of dithiothreitol to 5 mM and incubation at room temperature for 30 min. Cysteines were alkylated by adding iodoacetamide to 15 mM and incubating in the dark at room temperature for 60 min. Iodoacetamide was quenched with an additional 10 mM DTT. Samples were digested with lysyl endopeptidase (lysC) at 20 ng/μl overnight at room temperature after diluting the urea to 2 M by adding 3 volumes of 50 mM HEPES, pH 8.8. LysC-digested peptides were subsequently digested with trypsin at 15 ng/μl for 60 min at 37°C. Doubly digested peptides were acidified by adding trifluoroacetic acid to 0.2% and desalted on hand-packed C18 STAGE tips (Rappsilber *et al*, 2007). Peptides were eluted with 70% acetonitrile and 1% formic acid and dried under vacuum. Desalted peptides were resuspended in 5% formic acid, and each sample was analyzed in technical duplicate by reverse-phase liquid chromatography electrospray mass spectrometry on a LTQ Orbitrap Velos Pro (Thermo Fisher Scientific). Peptides were analyzed on a LTQ Orbitrap Velos Pro mass spectrometer (Thermo Fisher Scientific). Nanospray tips were hand-pulled with 100-μm inside diameter fused-silica tubing and packed with 20 cm of Maccel C18AQ resin (3 mm, 200 Å; Nest Group). Peptides were separated with a gradient of 6–30% CH3CN in 0.125% formic acid over 60 min at a flow rate of 300 nl/min. Peptides were detected using a data-dependent Top20 MS2 method. For each cycle, one full MS scan of mass/charge ratio (m/z) = 400–1,200 was acquired in the Orbitrap at a resolution of 60,000 at m/z = 400 with automatic gain control (AGC) target of 1×10^6. Each full scan was followed by the selection of the most intense ions, up to 20, for collision-induced dissociation (CID) and analysis in the linear ion trap. Selected ions were excluded from subsequent selection for 60 s. Ions with a charge of 1 or unassigned were also excluded from MS2 analysis. Maximum ion

accumulation times were 100 ms for both full MS and MS2 scans. Lockmass, with atmospheric polydimethylsiloxane (m/z = 371.1012) as an internal standard, was used for internal mass calibration.

Peptide identification and filtering

MS2 spectra were searched using SEQUEST v.28 (rev. 13) against a composite database containing the translated sequences of all predicted open reading frames of *S. cerevisiae* (http://downloads.yeastgenome.org, downloaded 30 October 2009) and its reversed complement with the following parameters: a precursor mass tolerance of ± 20 parts per million (ppm); 1.0-dalton product ion mass tolerance; combined lysC–trypsin digestion; up to two missed cleavages; a static modification of carbamidomethylation on cysteine (+57.0214); and a dynamic modifications of methionine oxidation (+15.9949). Peptide spectral matches were filtered to 1% FDR using the target-decoy strategy combined with linear discriminant analysis (LDA) using several different parameters including the SEQUEST Xcorr and DCn′ scores, and precursor mass error (Elias & Gygi, 2007; Huttlin *et al*, 2010). The data were further filtered to control protein-level FDRs. Peptides from all fractions in each experiment were combined and assembled into proteins. Protein scores were derived from the product of all LDA peptide probabilities, sorted by rank, and filtered to 1% FDR. The FDR of the remaining peptides fell markedly after protein filtering.

Steady-state protein analysis

Yeast whole-cell lysates were prepared from 1 OD_{600} of yeast cells harvested from raffinose medium at mid-log phase. Yeast pellets were washed with ddH_2O once, resuspended in 200 μl of 20 mM NaOH, incubated at room temperature for 5 min, and pelleted. Laemmli buffer was added to resuspend pellets, and they were denatured at 95°C for 5–10 min (Kushnirov, 2000). Anti-Cox2, Cox3 (MitoSciences), Por1, and Pgk1 (3-phosphoglycerate kinase) (Abcam) were used on immunoblots.

Animal tissue lysates were obtained from brain homogenates of 4- to 5-week-old wild-type and *ATAD1*$^{-/-}$ mice (C57BL/6) (Zhang *et al*, 2011). Freshly isolated whole brains were powderized on dry ice and homogenized in lysis buffer (50 mM HEPES, pH 7.5, 150 mM NaCl, 1 mM DTT, 5% glycerol, 1% Triton X-100) containing protease inhibitors (Sigma-Aldrich). The brain extracts were kept on ice for 1 h and then centrifuged at 15,000 × *g* for 30 min. Protein concentration was determined using the BCA protein assay (Thermo Scientific). Twenty μg of lysates was resolved on 4–20% gradient NuPAGE (Invitrogen) and transferred to PVDF membranes. Immunoblot analyses were performed using ATAD1 antibodies (NeuroMab or abcam) and mitochondrial antibodies, TOMM20, COX1, COX4, hexokinase 1, hexokinase 2, VDAC1, pyruvate dehydrogenase, and S6 ribosomal protein (Cell Signaling Tech.). β-actin, β-tubulin, and MAP2 (SIGMA) antibodies were used for controls. All mouse experiments were performed under approved protocols of the Institutional Animal Care and Use Committee at Johns Hopkins University School of Medicine.

Measurement of oxygen consumption rate

Mitochondrial oxygen consumption rate (OCR) was assessed using WT and *ATAD1* KO MEFs in an XF24 Extracellular Flux Analyzer (Seahorse Bioscience), as described previously (Cooper *et al*, 2012). Culture media of MEF cells plated at a density of ~0.5×10^6 per well in an XF24 cell culture microplates were replaced with XF24 Dulbecco's modified Eagle medium (DMEM) containing 10 mM glucose, 2 mM L-glutamine (Life Technologies), and 2 mM sodium pyruvate (Life Technologies). OCR was measured at 37°C with 1-min mix, 1-min wait, and 5-min measurement protocol. OCR was analyzed after 30 min incubation in a CO_2-free incubator. Oligomycin, carbonilcyanide m-chlorophenylhydrazone (CCCP), and rotenone were sequentially injected into each well to assess basal respiration, coupling of respiratory chain, and mitochondrial respiratory capacity. OCRs were normalized relative to protein concentration in each well, and the data are presented as % change of control.

Co-immunoprecipitation

One milligram of crude mitochondria extracted from each strain was solubilized in 0.5% digitonin for 1 h at 4°C. Cleared mitochondria lysates were mixed with anti-HA antibody-conjugated agarose for 1 h at 4°C. Agarose was washed two times with buffer containing 250 mM NaCl and 0.05% digitonin and three times with buffer containing 600 mM NaCl and 0.05% digitonin. Laemmli buffer without β-ME was added to the agarose to elute proteins. Final eluate and 4–5% of the mitochondria lysate were resolved by 12% SDS-PAGE followed by immunoblot. Results shown in this study are representatives of two independent experiments ($n = 2$).

Mammalian cell culture

HepG2 (human hepatocellular carcinoma) cells were maintained in DMEM/F12 (Thermo Scientific) with 10% FBS. HEK293T, HDF (human dermal fibroblasts), and HeLa cells were maintained in DMEM (Thermo Scientific) with 10% FBS. Cells were cultured at 37°C with 5% CO_2. To establish stable cell lines, retrovirus was produced in HEK293T cells that were co-transfected with the vector containing the gene of interest, Gag-pol, and VSVG (amount ratio is 3:2:1) using Lipofectamine 2000 (Invitrogen) according to the manufacturer's instructions. Retrovirus was harvested from the medium at 48 h post-transfection and applied to the target cells. After 24 h post-infection, target cells were selected in 4 μg/ml puromycin and/or 150 μg/ml zeocin for 5–7 days. Stable cell lines were maintained in the appropriate medium with 0.5 μg/ml puromycin and/or 20 μg/ml zeocin. All knockdowns were performed by treating cells with 10 nM siRNA, using the Lipofectamine RNAiMax reagent, according to the manufacturer's instructions (Invitrogen). The All-Stars non-targeting siRNA (Qiagen) was used as the control (scr). siRNAs targeting human *ATAD1* (NM_032810.2) were designed with the Dharmacon siDesign Center tool (http://www.thermoscientificbio.com/design-center/). Sequences of the sense strands of targeting siRNAs, which include a 3′ tt DNA overhang, are as follows: (#1) GAAGCAAAUUGGAGUGAAAtt, (#2) GAAUGAAGUUGUUGGUUUAtt, (3) CAUGUUACUUGGAGUGAUAtt and (4) GAUAAGUGGUAUGGAGAAUdtt. Cells were subjected to knockdown on day 0, again on day 3, and analyzed on day 6. Efficacy of *ATAD1* knockdown was verified by immunoblot with mouse monoclonal anti-ATAD1 antibody (1:1,000) (Abcam).

Mouse embryonic fibroblasts (MEFs) were prepared from embryonic day 13 mouse pups as described previously with some modification (Jozefczuk *et al*, 2012). MEFs were isolated from tissues by 0.05% trypsin/EDTA (Gibco, Invitrogen) dissociation. Cells were strained using 40-μm cell strainer (BD Falcon) and resuspended in Dulbecco's modified Eagle's medium (Gibco, Invitrogen), supplemented with 10% fetal bovine serum, 100 μg/ml penicillin, and 100 g/ml streptomycin. Cells were plated on poly-D-lysine-coated cell culture dishes. All mouse experiments were performed under approved protocols of the Institutional Animal Care and Use Committee at Johns Hopkins University School of Medicine.

Supplementary information for this article is available online: http://emboj.embopress.org

Acknowledgements

We thank members of the Rutter laboratory for helpful discussions; Tim Formosa, David Stillman, and Janet Shaw for yeast strains, reagents, antibodies, technical supports, and helpful discussions; Tammy Nguyen for assistance with mammalian live cell imaging; Adam Frost for discussing the MITO-MAP data and critical comments on the manuscript; Adam L. Hughes for critical comments on the manuscript; Dennis Winge for Sdh1 and Sdh2 antibodies. This work was supported by the NIH grant R01GM094232 (to J.R.) and the NIH/NIDA DA000266 (to T.M.D., V.L.D.) and NIH/NINDS 5R01AG029368 (to V.L.D.) American Heart Association 12SDG9310031 (S.A.A.). T.M.D. is the Leonard and Madlyn Abramson Professor in Neurodegenerative Diseases.

Author contributions

Y-CC and JR proposed project hypothesis, designed experiments and prepared manuscript. Y-CC performed and analyzed experiments of Figures 1, 2, 4, 5, 6 and Supplementary Figures 1-7. TMD, VLD, GKEU and SAA designed, performed and analyzed experiments of Figure 3. ND and SG performed mass spectrometry and analyzed the result.

Conflict of interest

The authors declare that they have no conflict of interest.

Note added in proof

In agreement with our conclusions, Okreglak and Walter (2014) independently demonstrated that yeast Msp1 promote the degradation of the mistargeted Pex15 tail-anchored protein on the mitochondrial outer membrane.

Okreglak V, Walter P (2014) The conserved AAA-ATPase Msp1 confers organelle specificity to tail-anchored proteins. *Proc Natl Acad Sci U S A*, in press

References

Ashrafi G, Schwarz TL (2013) The pathways of mitophagy for quality control and clearance of mitochondria. *Cell Death Differ* 20: 31 – 42

Boldogh IR, Pon LA (2007) Purification and subfractionation of mitochondria from the yeast *Saccharomyces cerevisiae*. *Methods Cell Biol* 80: 45 – 64

Borgese N, Colombo S, Pedrazzini E (2003) The tale of tail-anchored proteins: coming from the cytosol and looking for a membrane. *J Cell Biol* 161: 1013 – 1019

Brambillasca S, Yabal M, Soffientini P, Stefanovic S, Makarow M, Hegde RS, Borgese N (2005) Transmembrane topogenesis of a tail-anchored protein is modulated by membrane lipid composition. *EMBO J* 24: 2533 – 2542

Bricker DK, Taylor EB, Schell JC, Orsak T, Boutron A, Chen YC, Cox JE, Cardon CM, Van Vranken JG, Dephoure N, Redin C, Boudina S, Gygi SP, Brivet M, Thummel CS, Rutter J (2012) A mitochondrial pyruvate carrier required for pyruvate uptake in yeast, *Drosophila*, and humans. *Science* 337: 96 – 100

Campbell CL, Tanaka N, White KH, Thorsness PE (1994) Mitochondrial morphological and functional defects in yeast caused by yme1 are suppressed by mutation of a 26S protease subunit homologue. *Mol Biol Cell* 5: 899 – 905

Chartron JW, Suloway CJ, Zaslaver M, Clemons WM Jr (2010) Structural characterization of the Get4/Get5 complex and its interaction with Get3. *Proc Natl Acad Sci USA* 107: 12127 – 12132

Chen YC, Taylor EB, Dephoure N, Heo JM, Tonhato A, Papandreou I, Nath N, Denko NC, Gygi SP, Rutter J (2012) Identification of a protein mediating respiratory supercomplex stability. *Cell Metab* 15: 348 – 360

Cooper O, Seo H, Andrabi S, Guardia-Laguarta C, Graziotto J, Sundberg M, McLean JR, Carrillo-Reid L, Xie Z, Osborn T, Hargus G, Deleidi M, Lawson T, Bogetofte H, Perez-Torres E, Clark L, Moskowitz C, Mazzulli J, Chen L, Volpicelli-Daley L *et al* (2012) Pharmacological rescue of mitochondrial deficits in iPSC-derived neural cells from patients with familial Parkinson's disease. *Sci Transl Med* 4: 141ra190

Costanzo M, Baryshnikova A, Bellay J, Kim Y, Spear ED, Sevier CS, Ding H, Koh JL, Toufighi K, Mostafavi S, Prinz J, St Onge RP, VanderSluis B, Makhnevych T, Vizeacoumar FJ, Alizadeh S, Bahr S, Brost RL, Chen Y, Cokol M *et al* (2010) The genetic landscape of a cell. *Science* 327: 425 – 431

Denic V (2012) A portrait of the GET pathway as a surprisingly complicated young man. *Trends Biochem Sci* 37: 411 – 417

Dimmer KS, Fritz S, Fuchs F, Messerschmitt M, Weinbach N, Neupert W, Westermann B (2002) Genetic basis of mitochondrial function and morphology in *Saccharomyces cerevisiae*. *Mol Biol Cell* 13: 847 – 853

Elias JE, Gygi SP (2007) Target-decoy search strategy for increased confidence in large-scale protein identifications by mass spectrometry. *Nat Methods* 4: 207 – 214

Gerdes F, Tatsuta T, Langer T (2012) Mitochondrial AAA proteases–towards a molecular understanding of membrane-bound proteolytic machines. *Biochim Biophys Acta* 1823: 49 – 55

Gietz D, St Jean A, Woods RA, Schiestl RH (1992) Improved method for high efficiency transformation of intact yeast cells. *Nucleic Acids Res* 20: 1425

Goldstein AL, McCusker JH (1999) Three new dominant drug resistance cassettes for gene disruption in *Saccharomyces cerevisiae*. *Yeast* 15: 1541 – 1553

Hanson PI, Whiteheart SW (2005) AAA+ proteins: have engine, will work. *Nat Rev Mol Cell Biol* 6: 519 – 529

Hao HX, Khalimonchuk O, Schraders M, Dephoure N, Bayley JP, Kunst H, Devilee P, Cremers CW, Schiffman JD, Bentz BG, Gygi SP, Winge DR, Kremer H, Rutter J (2009) SDH5, a gene required for flavination of succinate dehydrogenase, is mutated in paraganglioma. *Science* 325: 1139 – 1142

Hegde RS, Keenan RJ (2011) Tail-anchored membrane protein insertion into the endoplasmic reticulum. *Nat Rev Mol Cell Biol* 12: 787 – 798

Heo JM, Livnat-Levanon N, Taylor EB, Jones KT, Dephoure N, Ring J, Xie J, Brodsky JL, Madeo F, Gygi SP, Ashrafi K, Glickman MH, Rutter J (2010) A stress-responsive system for mitochondrial protein degradation. *Mol Cell* 40: 465 – 480

Hessa T, Sharma A, Mariappan M, Eshleman HD, Gutierrez E, Hegde RS (2011) Protein targeting and degradation are coupled for elimination of mislocalized proteins. *Nature* 475: 394 – 397

Hoppins S, Collins SR, Cassidy-Stone A, Hummel E, Devay RM, Lackner LL, Westermann B, Schuldiner M, Weissman JS, Nunnari J (2011) A

mitochondrial-focused genetic interaction map reveals a scaffold-like complex required for inner membrane organization in mitochondria. *J Cell Biol* 195: 323 – 340

Huttlin EL, Jedrychowski MP, Elias JE, Goswami T, Rad R, Beausoleil SA, Villen J, Haas W, Sowa ME, Gygi SP (2010) A tissue-specific atlas of mouse protein phosphorylation and expression. *Cell* 143: 1174 – 1189

Janska H, Kwasniak M, Szczepanowska J (2013) Protein quality control in organelles – AAA/FtsH story. *Biochim Biophys Acta* 1833: 381 – 387

Jonikas MC, Collins SR, Denic V, Oh E, Quan EM, Schmid V, Weibezahn J, Schwappach B, Walter P, Weissman JS, Schuldiner M (2009) Comprehensive characterization of genes required for protein folding in the endoplasmic reticulum. *Science* 323: 1693 – 1697

Jozefczuk J, Drews K, Adjaye J (2012) Preparation of mouse embryonic fibroblast cells suitable for culturing human embryonic and induced pluripotent stem cells. *J Vis Exp* 3854

Karbowski M, Youle RJ (2011) Regulating mitochondrial outer membrane proteins by ubiquitination and proteasomal degradation. *Curr Opin Cell Biol* 23: 476 – 482

Kroemer G, Pouyssegur J (2008) Tumor cell metabolism: cancer's Achilles' heel. *Cancer Cell* 13: 472 – 482

Kushnirov VV (2000) Rapid and reliable protein extraction from yeast. *Yeast* 16: 857 – 860

Kutay U, Ahnert-Hilger G, Hartmann E, Wiedenmann B, Rapoport TA (1995) Transport route for synaptobrevin via a novel pathway of insertion into the endoplasmic reticulum membrane. *EMBO J* 14: 217 – 223

Lessing D, Bonini NM (2009) Maintaining the brain: insight into human neurodegeneration from *Drosophila melanogaster* mutants. *Nat Rev Genet* 10: 359 – 370

Longtine MS, McKenzie A III, Demarini DJ, Shah NG, Wach A, Brachat A, Philippsen P, Pringle JR (1998) Additional modules for versatile and economical PCR-based gene deletion and modification in *Saccharomyces cerevisiae*. *Yeast* 14: 953 – 961

Lopez-Armada MJ, Riveiro-Naveira RR, Vaamonde-Garcia C, Valcarcel-Ares MN (2013) Mitochondrial dysfunction and the inflammatory response. *Mitochondrion* 13: 106 – 118

Lopez-Otin C, Blasco MA, Partridge L, Serrano M, Kroemer G (2013) The hallmarks of aging. *Cell* 153: 1194 – 1217

Mariappan M, Li X, Stefanovic S, Sharma A, Mateja A, Keenan RJ, Hegde RS (2010) A ribosome-associating factor chaperones tail-anchored membrane proteins. *Nature* 466: 1120 – 1124

Mariappan M, Mateja A, Dobosz M, Bove E, Hegde RS, Keenan RJ (2011) The mechanism of membrane-associated steps in tail-anchored protein insertion. *Nature* 477: 61 – 66

McNew JA, Coe JG, Sogaard M, Zemelman BV, Wimmer C, Hong W, Sollner TH (1998) Gos1p, a *Saccharomyces cerevisiae* SNARE protein involved in Golgi transport. *FEBS Lett* 435: 89 – 95

Mumberg D, Muller R, Funk M (1995) Yeast vectors for the controlled expression of heterologous proteins in different genetic backgrounds. *Gene* 156: 119 – 122

Nakai M, Endo T, Hase T, Matsubara H (1993) Intramitochondrial protein sorting. Isolation and characterization of the yeast MSP1 gene which belongs to a novel family of putative ATPases. *J Biol Chem* 268: 24262 – 24269

Neutzner A, Youle RJ, Karbowski M (2007) Outer mitochondrial membrane protein degradation by the proteasome. *Novartis Found Symp* 287: 4 – 14; discussion 14-20

Noguchi T, Koizumi M, Hayashi S (2011) Sustained elongation of sperm tail promoted by local remodeling of giant mitochondria in *Drosophila*. *Curr Biol* 21: 805 – 814

Patti ME, Corvera S (2010) The role of mitochondria in the pathogenesis of type 2 diabetes. *Endocr Rev* 31: 364 – 395

Rappsilber J, Mann M, Ishihama Y (2007) Protocol for micro-purification, enrichment, pre-fractionation and storage of peptides for proteomics using StageTips. *Nat Protoc* 2: 1896 – 1906

Rugarli EI, Langer T (2012) Mitochondrial quality control: a matter of life and death for neurons. *EMBO J* 31: 1336 – 1349

Sauer RT, Baker TA (2011) AAA+ proteases: ATP-fueled machines of protein destruction. *Annu Rev Biochem* 80: 587 – 612

Schuldiner M, Metz J, Schmid V, Denic V, Rakwalska M, Schmitt HD, Schwappach B, Weissman JS (2008) The GET complex mediates insertion of tail-anchored proteins into the ER membrane. *Cell* 134: 634 – 645

Steel GJ, Brownsword J, Stirling CJ (2002) Tail-anchored protein insertion into yeast ER requires a novel posttranslational mechanism which is independent of the SEC machinery. *Biochemistry* 41: 11914 – 11920

Stefanovic S, Hegde RS (2007) Identification of a targeting factor for posttranslational membrane protein insertion into the ER. *Cell* 128: 1147 – 1159

Tanaka A, Cleland MM, Xu S, Narendra DP, Suen DF, Karbowski M, Youle RJ (2010) Proteasome and p97 mediate mitophagy and degradation of mitofusins induced by Parkin. *J Cell Biol* 191: 1367 – 1380

Taylor EB, Rutter J (2011) Mitochondrial quality control by the ubiquitin-proteasome system. *Biochem Soc Trans* 39: 1509 – 1513

Thorsness PE, White KH, Fox TD (1993) Inactivation of YME1, a member of the ftsH-SEC18-PAS1-CDC48 family of putative ATPase-encoding genes, causes increased escape of DNA from mitochondria in *Saccharomyces cerevisiae*. *Mol Cell Biol* 13: 5418 – 5426

Tokuyasu KT (1975) Dynamics of spermiogenesis in *Drosophila melanogaster*. VI. Significance of "onion" nebenkern formation. *J Ultrastruct Res* 53: 93 – 112

Wach A, Brachat A, Pohlmann R, Philippsen P (1994) New heterologous modules for classical or PCR-based gene disruptions in *Saccharomyces cerevisiae*. *Yeast* 10: 1793 – 1808

Wang F, Brown EC, Mak G, Zhuang J, Denic V (2010) A chaperone cascade sorts proteins for posttranslational membrane insertion into the endoplasmic reticulum. *Mol Cell* 40: 159 – 171

Wattenberg B, Lithgow T (2001) Targeting of C-terminal (tail)-anchored proteins: understanding how cytoplasmic activities are anchored to intracellular membranes. *Traffic* 2: 66 – 71

Weibezahn J, Schlieker C, Bukau B, Mogk A (2003) Characterization of a trap mutant of the AAA+ chaperone ClpB. *J Biol Chem* 278: 32608 – 32617

Xu S, Peng G, Wang Y, Fang S, Karbowski M (2011) The AAA-ATPase p97 is essential for outer mitochondrial membrane protein turnover. *Mol Biol Cell* 22: 291 – 300

Yabal M, Brambillasca S, Soffientini P, Pedrazzini E, Borgese N, Makarow M (2003) Translocation of the C terminus of a tail-anchored protein across the endoplasmic reticulum membrane in yeast mutants defective in signal peptide-driven translocation. *J Biol Chem* 278: 3489 – 3496

Youle RJ, Narendra DP (2011) Mechanisms of mitophagy. *Nat Rev Mol Cell Biol* 12: 9 – 14

Zhang J, Wang Y, Chi Z, Keuss MJ, Pai YM, Kang HC, Shin JH, Bugayenko A, Wang H, Xiong Y, Pletnikov MV, Mattson MP, Dawson TM, Dawson VL (2011) The AAA+ ATPase Thorase regulates AMPA receptor-dependent synaptic plasticity and behavior. *Cell* 145: 284 – 299

